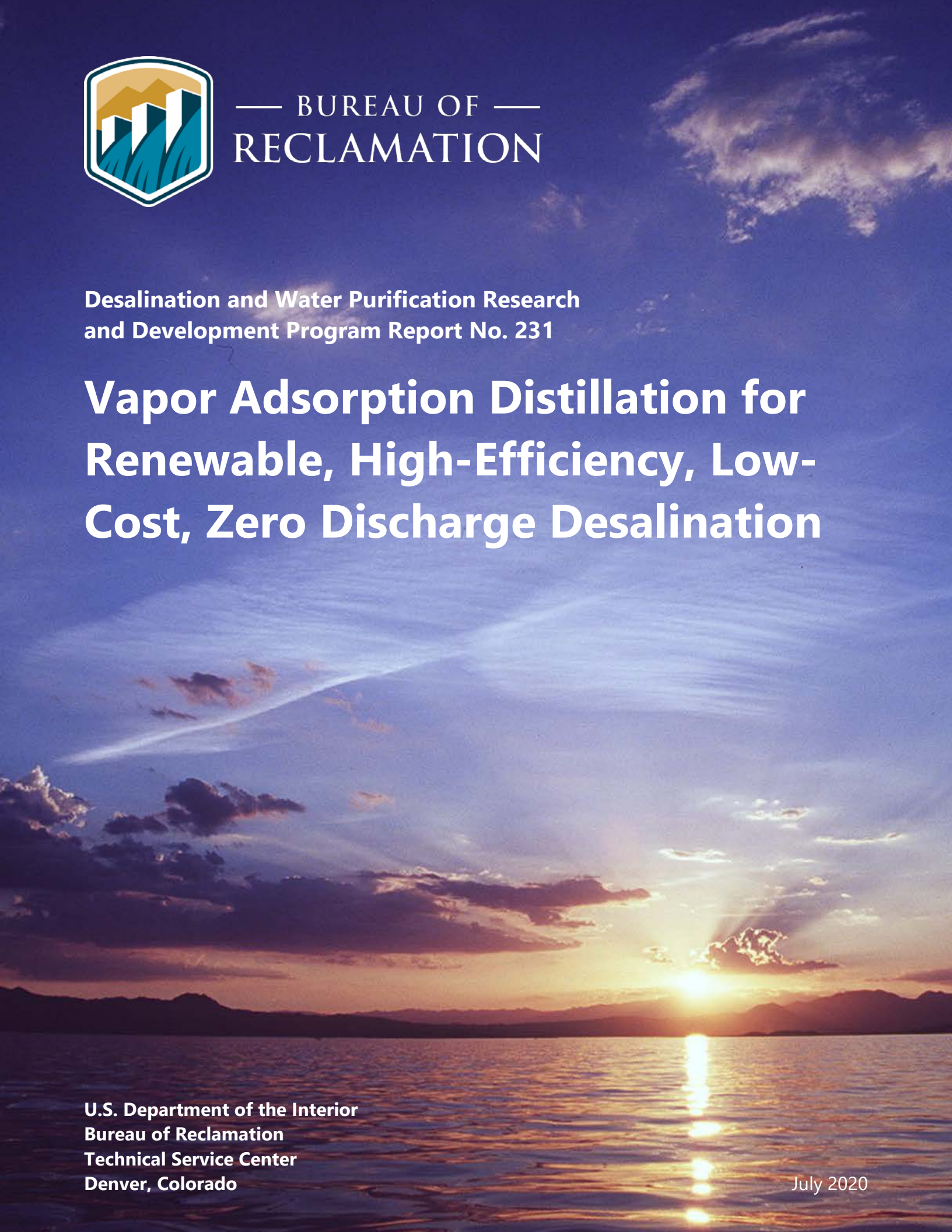

BUREAU OF RECLAMATION

Desalination and Water Purification Research and Development Program Report No. 231

Vapor Adsorption Distillation for Renewable, High-Efficiency, Low-Cost, Zero Discharge Desalination

U.S. Department of the Interior
Bureau of Reclamation
Technical Service Center
Denver, Colorado

July 2020

REPORT DOCUMENTATION PAGE

Form Approved
OMB No. 0704-0188

1. REPORT DATE *(DD-MM-YYYY)*	2. REPORT TYPE	3. DATES COVERED *(From - To)*
30-09-2019	Final	From ___ to 30-09-2019

4. TITLE AND SUBTITLE
Vapor Adsorption Distillation for Renewable, High-Efficiency, Low-Cost, Zero Discharge Desalination

5a. CONTRACT NUMBER
Agreement No. R17AC00146

5b. GRANT NUMBER

5c. PROGRAM ELEMENT NUMBER

6. AUTHOR(S)
Howard Yuh, CEO, Senior Scientist
Ethan Schartman, CTO, Senior Scientist
Kevin Tritz, COO, Senior Scientist

5d. PROJECT NUMBER

5e. TASK NUMBER

5f. WORK UNIT NUMBER

7. PERFORMING ORGANIZATION NAME(S) AND ADDRESS(ES)
GreenBlu, Inc.
1800 East State Street, Suite 145
Hamilton, NJ 08609

8. PERFORMING ORGANIZATION REPORT NUMBER

9. SPONSORING/MONITORING AGENCY NAME(S) AND ADDRESS(ES)
Bureau of Reclamation
U.S. Department of the Interior
Denver Federal Center
PO Box 25007, Denver, CO 80225-0007

10. SPONSOR/MONITOR'S ACRONYM(S)
Reclamation

11. SPONSOR/MONITOR'S REPORT NUMBER(S)
DWPR Report No. 231

12. DISTRIBUTION/AVAILABILITY STATEMENT
Available from the National Technical Information Service,
Operations Division, 5285 Port Royal Road, Springfield VA 22161

13. SUPPLEMENTARY NOTES
Online at https://www.usbr.gov/research/dwpr/DWPR_Reports.html

14. ABSTRACT
This project advances research in multiple-effect adsorption distillation, a method patented by GreenBlu, Inc. that recycles both the latent heat of vaporization and the heat of adsorption. A composite adsorbent material with improved thermal properties was developed and tested in a prototype single-effect distiller. Water adsorption/desorption distillation was demonstrated along with preliminary zero-liquid discharge (ZLD) capabilities using this technique. These results support the feasibility of large-scale commercial desalination and ZLD using solar/waste heat-driven adsorption distillation.

15. SUBJECT TERMS
Desalination, adsorption, multiple-effect, zero liquid discharge, renewable, solar, waste heat

16. SECURITY CLASSIFICATION OF:			17. LIMITATION OF ABSTRACT	18. NUMBER OF PAGES	19a. NAME OF RESPONSIBLE PERSON
a. REPORT	b. ABSTRACT	THIS PAGE	U		Andrew Tiffenbach
U	U	U			19b. TELEPHONE NUMBER *(Include area code)* (303) 445-2392

Desalination and Water Purification Research and Development Program Report No. 231

Vapor Adsorption Distillation for Renewable, High-Efficiency, Low-Cost, Zero Discharge Desalination

Prepared for the Bureau of Reclamation Under Agreement Number R17AC00146

by:

Dr. Howard Yuh, CEO and Senior Scientist
Dr. Ethan Schartman, CTO and Senior Scientist
Dr. Kevin Tritz, COO and Senior Scientist

GreenBlu, Inc.

Mission Statements

The Department of the Interior conserves and manages the Nation’s natural resources and cultural heritage for the benefit and enjoyment of the American people, provides scientific and other information about natural resources and natural hazards to address societal challenges and create opportunities for the American people, and honors the Nation’s trust responsibilities or special commitments to American Indians, Alaska Natives, and affiliated island communities to help them prosper.

The mission of the Bureau of Reclamation is to manage, develop, and protect water and related resources in an environmentally and economically sound manner in the interest of the American public.

Disclaimer

The views, analysis, recommendations, and conclusions in this report are those of the authors and do not represent official or unofficial policies or opinions of the United States Government, and the United States takes no position with regard to any findings, conclusions, or recommendations made. As such, mention of trade names or commercial products does not constitute their endorsement by the United States Government.

Acknowledgements

This research was sponsored by the Bureau of Reclamation’s Desalination and Water Purification Research and Development Program.

Acronyms and Abbreviations

Acronym or Abbreviation	Definition
MED	multiple effect distillation
MGD	million gallons per day
NASA	National Aeronautics and Space Administration
NPT	national pipe thread
PID	proportional integral derivative
RO	reverse osmosis
ZLD	zero liquid discharge

Measurements

Unit	Measurement
°C	degrees Celsius
$Ca_3(PO_4)_2$	calcium phosphate
$CaSO_4$	calcium sulfate
cm	centimeter
°F	degrees Fahrenheit
K	degrees Kelvin
km^3/year	cubic kilometers per year
kWh	kilowatt hour
kWh/m^3	kilowatt hours per cubic meter
m^3/day	cubic meters per day
$Mg(OH)_2$	magnesium hydroxide
NaCl	sodium chloride
µg/L	microgram per liter
W/(m*K)	watts per meter-Kelvin

Table of Contents

Acronyms and Abbreviations ..... **i**

Measurements ..... **ii**

Executive Summary ..... **vii**

1 Introduction **1**

1.1 Project Background 1

1.1.1 Problem 1

1.1.2 Participants/Prior Work 4

1.2 Project Needs and Objectives 5

1.2.1 Needs 5

1.2.2 Objectives 5

1.3 Project Overview 6

1.3.1 Overall Approach and Concepts 6

1.3.2 Overall Method 8

2 Technical Approach and Methods **11**

2.1 Project Facility/Physical Apparatus 11

2.1.1 Design Criteria 11

2.1.2 Source Water 11

2.1.3 Set-Up 11

2.2 Methodology 12

2.2.1 Methods Used 12

2.3 Analysis 15

2.3.1 Analytical Background 15

2.3.2 Analytical Process 17

3 Results and Discussion **19**

3.1 Measured Adsorbent Thermal Conductivities 19

3.2 Comparing Measured Permeability with Models 20

3.3 Adsorbent Module Fabrication Techniques 20
3.4 Adsorbent Bed Proof-of-Concept Prototype 22
3.5 Adsorbent Bed Test Stand 24
3.5.1 Vapor Uptake Kinetics Testing 26
3.6 Adsorbent Bed Proof-of-Concept Design and Construction 29
4 Conclusions and Recommendations 31
4.1 Conclusions 31
4.2 Recommended Next Steps 32
References 33
Metric Conversions 35

List of Figures

Figure 1. GreenBlu's envisioned commercial product is a grid-independent, solar thermal-powered, containerized module using 410 m^2 of solar collection that produces 16,000 gallons/day (60 m^3/day) 3
Figure 2. Schematic of proposed multiple-effect adsorption distiller 8
Figure 3. Vapor permeability testing apparatus as designed in CAD (top), and operational as-built (bottom) 12
Figure 4. Annular adsorbent samples fabricated for permeability testing 13
Figure 5. Thermal testing apparatus 14
Figure 6. Adsorbent test sample thermal conductivity vs. graphite density 19
Figure 7. Adsorbent test sample vapor permeability vs. density with marker size related to adsorbent average particle size 21
Figure 8. Adsorbent module fabrication progress: a) improved compressing and curing molds; b) initial unsuccessful attempts; and c) modules after multiple cycles in prototype 22
Figure 9. Completed proof-of-concept adsorbent bed with evaporator and condenser 23
Figure 10. Prototype adsorbent bed connected to test stand 24

Figure 11. Equilibrium vapor pressure vs. temperature and uptake data from the adsorbent bed 25

Figure 12. Completed adsorption bed connected to the test stand successfully distilling saturated NaCl brine using low-grade heat 26

Figure 13. Adsorbent module uptakes kinetics testing apparatus 27

Figure 14. Updated approach to balancing vapor uptake testing chamber. Careful calibration and suspension from center of mass on each scale will eliminate influence of torques in the system on water mass measurements. 28

Figure 15. Temperature changes during an initial test of the uptake kinetics testing chamber 29

Figure 16. Conceptual design and rendering of commercial adsorption distiller 30

List of Tables

Table 1. Adsorbent constituents used to calculate densities 17

Table 2. Key specifications of the conceptual design 32

This page intentionally left blank.

Executive Summary

Freshwater scarcity is a global issue, with 4 billion people (two-thirds of the global population) impacted by severe water scarcity for at least 1 month of each year, and 500 million people facing such conditions throughout the year (Mekonnen and Hoekstra 2016). According to the U.S. Government Accountability Office, 40 of 50 state water managers expect water shortages in some portion of their states over the next decade (GAO 2014). Clearly, there is a tremendous need for new safe and effective technologies for providing potable freshwater. Current methods of desalinating water face high costs, high energy use, and high environmental impact due to greenhouse gas emissions and intense brine discharge (Water in the West 2016; Tularam and Ilahee 2007; LIGTT 2014).

As desalination becomes an increasingly important tool to alleviate water scarcity, it is important to address its environmental impacts, including brine discharge and carbon-intensity. Existing membrane and electrodialysis techniques are efficient desalination techniques, with the most advanced installations reaching within a factor of two of the ideal thermodynamic separation energy. Although advances in thermally-powered techniques have lagged in recent years, improvements may be highly complementary to the aforementioned techniques, including the ability to optimize both first- and second-law efficiencies with lower exergy waste or solar heat, and the ability to completely eliminate waste brine.

Thermal techniques are generally known to function better than membrane or electrodialysis techniques at high salinities because vapor pressure is a weak function of salinity. However, drawbacks include the inability to improve efficiency through the use of higher temperatures due to the top brine temperature and the lack of efficient thermal crystallizers to enable zero-liquid-discharge products.

This project advances research in multiple-effect adsorption distillation, a method patented by GreenBlu, Inc., that recycles both the latent heat of vaporization and the heat of adsorption. Using an adsorbent intermediary in the distillation process, input heat is no longer limited by the top brine temperature because the adsorbent replaces the brine as the highest-temperature component, allowing adsorption distillation to make use of economical exergy at mid-range temperatures between 100 and 200°C. An efficient crystallizer can be designed using the solid-state adsorption vapor pump.

GreenBlu envisions products resulting from this research to include solar- and waste-heat powered distillers and crystallizers. The products are modular and containerized but can be unloaded and rack-mounted in a building for large installations. Each 40-foot shipping container module will make 16,000 gallons a day. A train carrying 63 units desalinates 1 million gallons per day (MGD), enough for a town. Solar heat for a 1-MGD plant only requires shading a 10-acre parking lot.

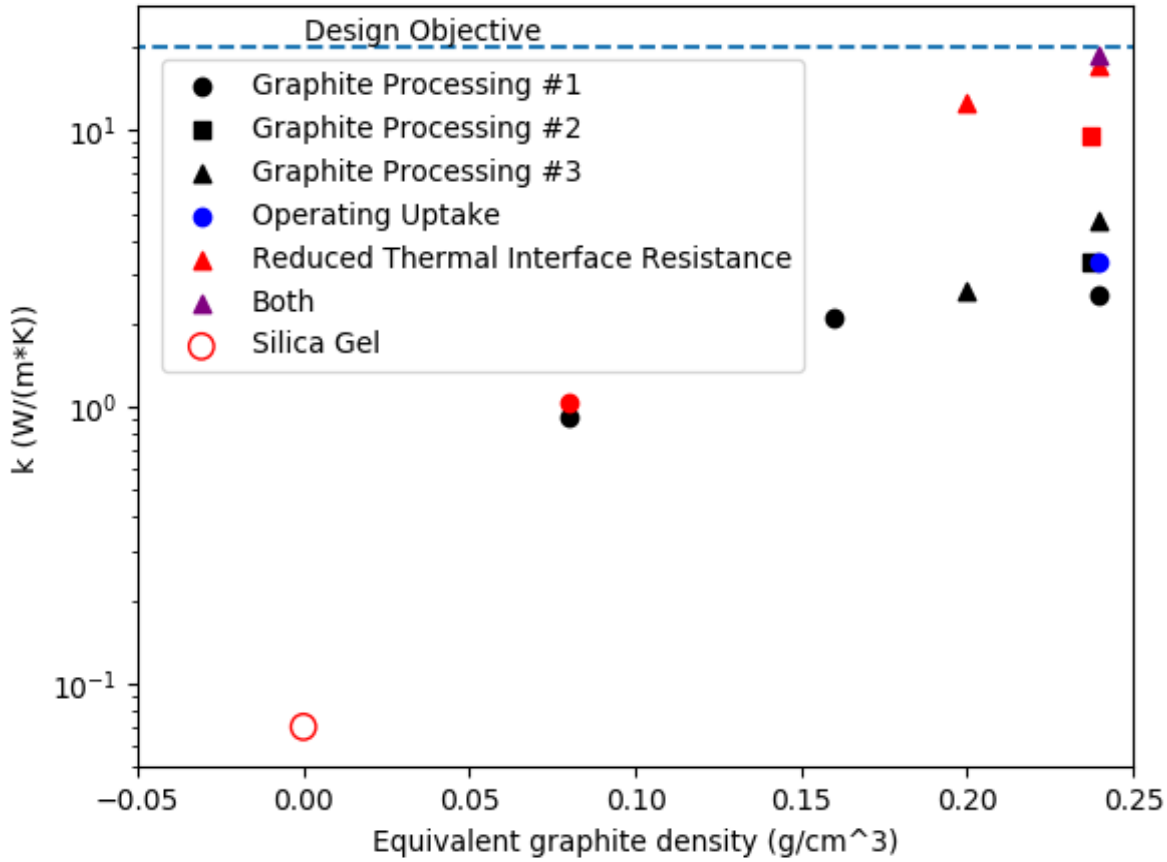

Figure ES-1. Adsorbent test sample thermal conductivity vs. graphite density

One of the primary objectives of this project was to optimize the adsorbent recipe and manufacturing technique to deliver a high-thermal-performance adsorbent rod module with sufficient thermal conductivity and vapor permeability to meet our water-cycle production goals. We were able to refine the graphite processing technique to increase the thermal conductivity of the adsorbent by a factor of about two while also identifying the graphite content needed for a commercial product thermal conductivity design objective of 20 W/(m*K). Figure ES-1 shows the measured thermal conductivity of our adsorbent samples with the measurement and analysis methodology described in more detail in Sections 2 and 3.

Vapor permeability is another adsorbent property that needs to be optimized along with thermal conductivity. We designed and built a custom permeability test stand and measured vapor permeability as a function of adsorbent properties such as particle size and density. The results from these measurements are shown in Figure ES-2, with additional details regarding methodology described in Sections 2 and 3.

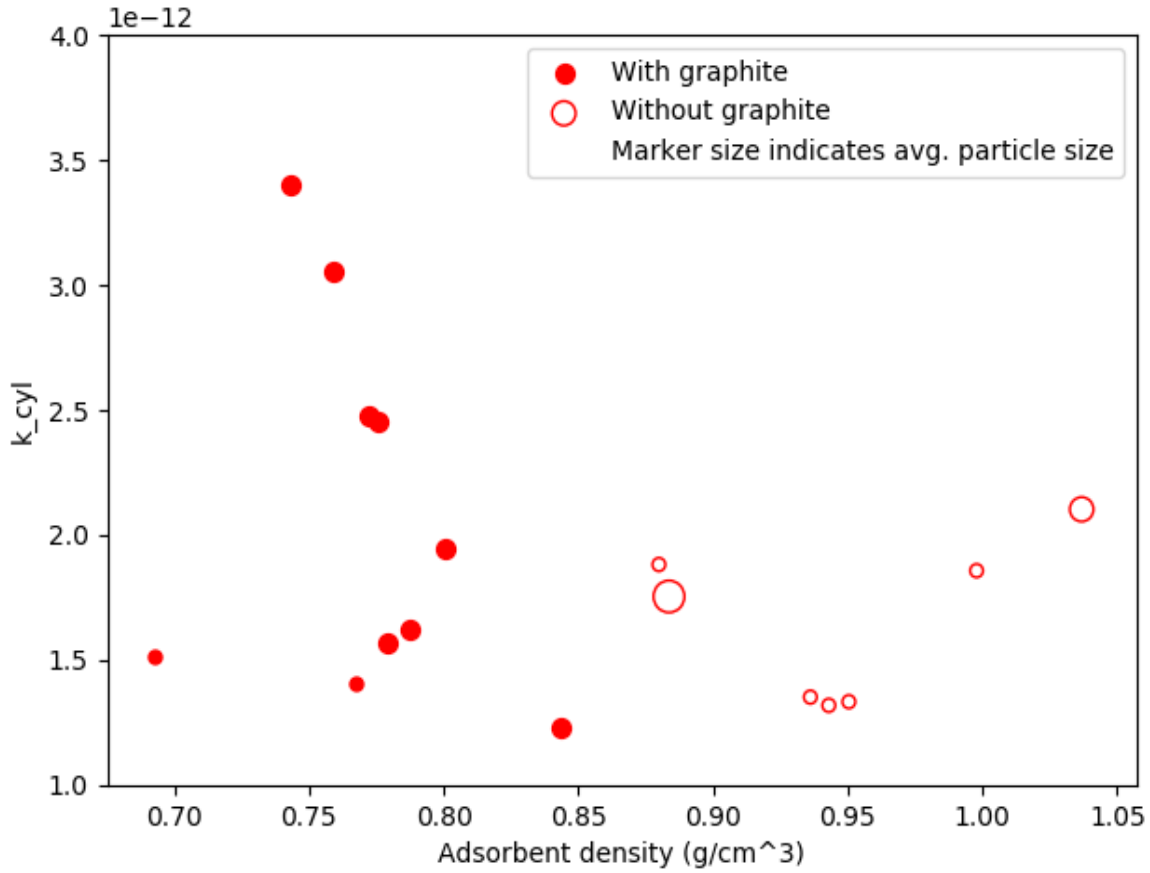

Figure ES-2. Adsorbent test sample vapor permeability vs. density with marker size related to adsorbent average particle size

This page intentionally left blank.

1 Introduction

1.1 Project Background

1.1.1 Problem

1.1.1.1 Increasing Water Scarcity

Fourteen of the world's largest cities (with populations in excess of 10 million) and two-fifths of cities with populations between 1 million and 10 million are located in coastal areas (Tibbetts 2002). Because 97.5 percent of the earth's water is saltwater, seawater desalination is a useful technology for addressing water scarcity problems in coastal regions (SBC 2014). For decades, desalination operations in many countries in the Middle East, the Mediterranean Basin, Australia, and the United States have provided drinking water to their populations (Kim et al. 2015). However, current methods cannot be expanded greatly without detrimental effect. Seawater desalination is saddled with high cost, high energy use, and high environmental impact due to greenhouse gas emissions and intense brine discharge (Water in the West 2016; Tularam and Ilahee 2007; LIGTT 2014). Reverse osmosis requires the use of chemical disinfection, both before and after desalination, resulting in harmful disinfection by-product formation, in part due to due to high levels of bromide and iodide in seawater (Kim et al. 2015).

Even while California has been experiencing its worst drought in centuries, leading experts who gathered at Woods Institute for the Environment at Stanford reached the consensus that ocean desalination based on current reverse osmosis (RO) technology is unlikely to ever contribute significantly to California's water supply, largely due to the pain points of cost, energy use, and environmental impact (Water in the West 2016).

The number of water-stressed people is projected to reach more than 5 billion by 2050 (Roberts 2014); however, desalination practices around the world are expected to expand in efforts to meet water needs. Global production of desalinated water has grown from approximately 65.2 million cubic meters per day (m3/day) in 2012 (IEA-ETSAP and IRENA 2012) to 95.4 million m3/day in 2018 (Jones et al. 2019). In 2012, desalination provided 0.6 percent of total water supplies but consumed 0.4 percent of total electricity (IEA-ETSAP and IRENA 2012).

The 2030 Water Resources Group reported that by 2030, global water demand will grow from 4,500 cubic kilometers per year (km3/year) to 6,900 km3/year, but only 4,200 km3/year is reliably sustainable (2030 Water Resources Group 2016). As much as 33 percent of all water withdrawals is currently unsustainably supplied using fossil groundwater, but global aquifer depletion rates measured by the National Aeronautics and Space Administration's (NASA)

GRACE satellites show the risks of depleting this resource (Famiglietti 2014) as climate change introduces more precipitation variability.

Water scarcity immediately translates into higher food and textile pricing, increasing suffering and conflict (SBC 2014). Because desalination requires large amounts of energy, often derived from fossil fuels, the process is subject to volatile market prices and lacks sustainability (IEA-ETSAP and IRENA 2012). Currently, only 1 percent of total desalinated water is produced via renewable energy sources (IEA-ETSAP and IRENA 2012).

1.1.1.2 Issues with Current Desalination Methods

Facilities using efficient methods for desalination, such as RO, are currently electrically powered and designed for continuous operation. To power these types of facilities using renewable resources requires both generation and significant storage of electricity to accommodate the intermittent nature of solar or wind power. Furthermore, large scale-up of electricity-intensive desalination will necessarily slow the overall decarbonization of the world's power production.

A fraction of the developing world will likely need desalination before centralized water and electric grid buildouts; therefore, a distributed solution is needed. For these reasons, the Institute for Globally Transformative Technologies at Lawrence Berkeley National Laboratory ranked scalable, low cost, and renewable-energy-powered desalination as the most urgently needed breakthrough necessary for sustainable development out of 50 urgent technologies (LIGTT 2014). Ideally, a solution could be found that can be powered using renewable energy but does not require electricity, does not generate brine waste, can be modularized for use in a distributed water network, and be cost-effective.

With increasing use of desalination, brine disposal is becoming an increasingly important long-term issue. A United Nations University paper reports that in 2018, brine discharge from nearly 16,000 desalination plants reached 141.5 million m3/day, enough to cover all of Florida in 1 foot of brine each year (Jones et al. 2019). Almost 80 percent of brine is produced along coastlines, and the risks of increased salinity, toxic chemicals containing copper and chlorine in the form of anti-scalants and anti-foulants, and oxygen depletion over the long term need to be considered. The authors point out that new technology should be developed that can transform waste brine into useful minerals that are contained in seawater brine.

1.1.1.3 RO vs. Thermal Distillation

Distillation offers advantages at high salinity because the additional energy required to separate water from a salt solution can come from a heat source rather than electricity. The efficiency of pressure-driven membrane processes at low salinities becomes a disadvantage at high salinity as osmotic pressures rapidly rise. All commercial membranes are unable to withstand the osmotic pressures of saturated brine at 380 bars, compared to the 70 to 85 bars used for seawater desalination (Thiel et al. 2015). In contrast, the vapor pressure of brine only modestly increases with salinity, which can be compensated by a small increase in brine temperature. RO becomes

increasingly inefficient as salinities approach saturation because even as the pressure dramatically increases, the recovery ratio decreases due to the inability to handle salt precipitation fouling at the membrane (Thiel et al. 2015). Electrodialysis systems are also most efficient at low salinities because the process acts on ions. As ionic concentration increases, it also becomes cost-disadvantageous to supply the additional energy of separation as electricity.

However, thermal systems typically struggle to fully recycle the large latent heats (627 kWh/m3) before exergy exhaustion. The latent heat and the heat of adsorption are much larger than the work of separation, which can range from 1.06 kWh/m3 for 50 percent recovery from seawater to 7.7 kWh/m3 for recovery of water from saturated NaCl solution Vane 2017). However, existing thermal distillers are also not able to deal with solutions near saturation because of scaling on the heat transfer surfaces. Many limitations with current distillation techniques stem from the fact that film and flash evaporation are highly susceptible to scaling.

1.1.1.4 Adsorption Distillation as a Solution

GreenBlu was founded to advance and commercialize a technology that could potentially address all of these difficult requirements. GreenBlu has patented a desalination device with a multiple-effect adsorption cycle that could achieve a breakthrough in thermal efficiency and zero liquid discharge (ZLD) functionality. This cycle will be driven by solar heat, or alternatively, for large installations, industrial waste heat. Modular units will be packaged and deployed in standard shipping containers for scalability and modularity (see Figure 1). Our technique solves long-standing issues with thermal distillation of seawater, such as top brine temperatures, and design features to minimize mineral scaling are being incorporated.

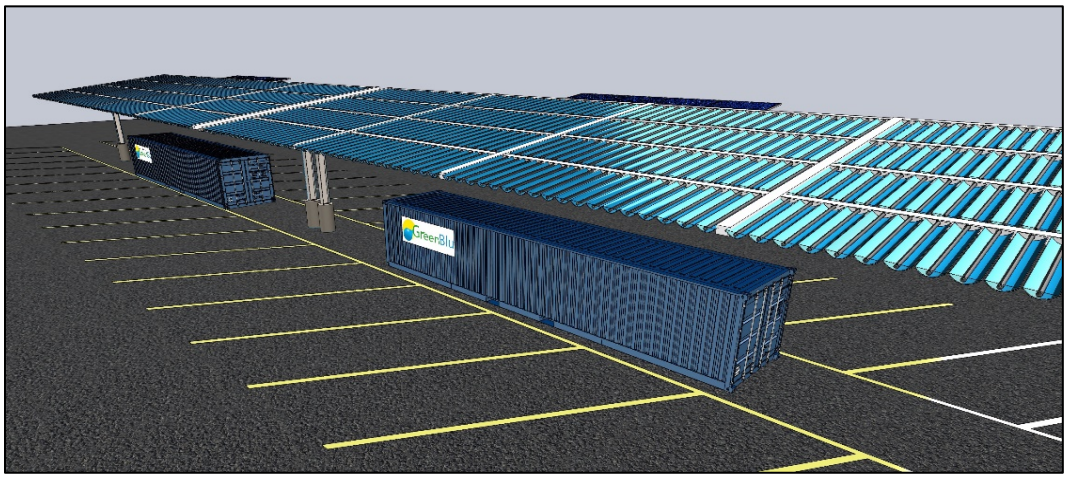

Figure 1. GreenBlu's envisioned commercial product is a grid-independent, solar thermal-powered, containerized module using 410 m^2 of solar collection that produces 16,000 gallons/day (60 m^3/day)

Multiple-effect adsorption has the potential to triple first-law energy efficiency through the use of the exergy in higher-grade heat because it is able to bypass top brine temperature limits using adsorbents. GreenBlu improves efficiency by combining three novel technologies: 1) a

composite nanomaterial adsorbent that enables a new adsorption distillation cycle, 2) a novel adsorption distillation cycle efficient enough to enable the use of solar thermal energy, and 3) low-cost, low-concentration solar collection.

GreenBlu's novel adsorbent, adsorption cycle, and solar collection solve the issue of energy intensity, yielding high-areal water production at low costs. The same technology will power a crystallizer that can make many ZLD applications economically viable by generating revenue from fresh water, brine disposal, and mineral recovery.

1.1.2 Participants/Prior Work

Silica gel is used as a highly porous matrix for a hygroscopic (water absorbing) salt. This composite of salt impregnated in the internal pore surfaces of mesoporous silica gel has been studied since its discovery in 1996 by Aristov, who called it a Selective Water (ad)Sorbent (Aristov et al. 1996). Confining a hygroscopic salt within silica gel pores more than doubles the adsorbed water mass per mass of adsorbent above just silica gel by allowing chemisorption in addition to physical adsorption. Using the pores of the silica gel combines the advantages of both liquid desiccant and solid-state adsorbents.

Adsorption heat pumps based on silica gel are viable products, including prototypes at Oak Ridge National Laboratory and at least one commercial product from PPI called Eco-Max. However, silica gel is a thermal insulator, and the low thermal conductivity can quickly slow or stop the adsorption process if the heat of adsorption is not effectively removed. Previous attempts by Freni et. al. using bentonite clay to couple the silica gel with finned metal heat sinks (Freni et al. 2007) proved to be not effective enough for our design, because the adsorption distiller relies on small temperature differentials using inexpensive materials.

GreenBlu has previously fabricated a three-component adsorbent consisting of silica gel, a hygroscopic salt, and graphite. Compression of this adsorbent enhances thermal conductivity sufficiently to allow heat to be efficiently transferred to and from the adsorbent. The current project builds on this previous work to develop the adsorbent into a commercial product.

GreenBlu seeks to use this adsorbent in a multiple-effect adsorption distiller consisting of a number of open-cycle adsorption stages connected in series, in which the exhaust heat from an upper stage is used to drive the next stage. By eliminating the heat-pumping action to maximize the number of stages, a 16-effect distiller is estimated to be possible using mid-grade heat. Based on an extensive literature and patent search, ours will be the first use of this method.

In contrast with an adsorption heat pump used to lower the bottom brine temperature to extend a Multiple-Effect Distillation (MED) stack (Thu et al. 2015) in an adsorption distiller, all water is produced through adsorption. The evaporator and condenser are kept essentially isothermal using a high heat transfer coefficient flat-plate condenser/evaporator, thereby minimizing the temperature difference needed to drive each stage. Similarly, the number of thermal transfers required between adsorbent within serial stages necessitates the use of high thermal-conductivity

media. The evaporator/condenser design also isolates brine contact to only the flat-plate evaporator, which is amenable to both in-situ scale removal methods and is easily disassembled and cleaned, mitigating the maintainability issue common to extended heat transfer surfaces in distillation plants.

1.2 Project Needs and Objectives

1.2.1 Needs

1.2.1.1 Adsorbent Development

GreenBlu has identified a promising novel composite nanomaterial that can enable a multiple-effect adsorption cycle. Current water adsorbents, including silica gel, zeolites, and metal organic frameworks, are insulators. In order to recycle the heat of adsorption, highly conducting thermal properties must be achieved in the adsorbent. The enabling composite material has been fabricated in small quantities and is not yet suitable for a commercial product.

1.2.1.2 Adsorption Bed Prototype

The adsorption bed design needed for GreenBlu's distiller has never been designed or prototyped before. It is necessary to construct a proof-of-concept benchtop-sized device to determine if such a device can be constructed.

1.2.2 Objectives

This project focuses on five key research and development goals as outlined below.

1. Adsorbent recipe optimization: The adsorbent composition contains several constituents with varying characteristics, and the weight fraction of each constituent needs to be optimized for the properties needed in the adsorbent material, including:
   a. water uptake;
   b. thermal conductivity;
   c. vapor permeability; and
   d. mechanical stability.
2. Adsorbent manufacturing techniques: For use in a commercial product, the granular adsorbent must be manufactured into a stable form factor that is mechanically sound yet maintains the attractive properties. Heat transfer tubing must be embedded within the adsorbent modules and maintain good thermal contact while not suffering corrosion. The adsorbent will be optimized and developed into a form factor capable of executing a multiple-effect adsorption distiller as part of this project.
3. Prototype adsorption beds: An adsorption bed prototype will be designed and constructed that allows the necessary vapor and fluid flow paths needed for distillation of the input fluid and the concentration/dewatering of the brine.

4. Conceptual design of commercial product: A multiple-effect adsorption distiller using a high thermal performance adsorbent has never been executed before. A prototype adsorption bed and a commercial multiple-effect distiller conceptual design will be completed as part of this project.
5. Conduct customer interview for pilot, beachhead, municipal, and desalination markets: Stakeholder interviews must be conducted at the development stage to assess the needs of the market and desirable features of a commercial product.

1.3 Project Overview

1.3.1 Overall Approach and Concepts

The proposed project uses an adsorbent intermediary to solve some long-standing issues with thermal distillation, such as the top brine temperature limit and the inability to perform ZLD functions. However, to achieve a net gain in efficiency, significant development must go into both the adsorbent and the distillation cycle.

The top brine limit arises from the inverse solubility of several scaling compounds, such as $CaSO_4$, $Mg(OH)_2$, and $Ca_3(PO_4)_2$ (Al-Ahmad and Aleem 1993). The scaling from these salts on heat transfer surfaces typically limits the highest temperature seawater can be heated to below 120ºC, depending on the anti-scaling chemicals used and whether the input water is pretreated using micro/nano-filtration to partially remove salt ions. The adsorption distiller overcomes the top brine limit because the adsorbent is operated above the brine temperatures, allowing higher-temperature input heat to drive more stages even while the temperature of the seawater remains below the scaling temperature. Also, because the evaporator is operated as a pool boiler rather than a film evaporator, local scaling, where local concentration limits are violated due to excessive local evaporation, should have reduced severity.

Solar desalination must achieve high-areal productivity (volume of water per square meter) to be viable. In practice, this translates into both first- and second-law efficiency (i.e., in energy [Joules] and in exergy [Joules]). Low concentration is a cost-effective and efficient means of boosting the temperature, hence the exergy of solar heat, but the top brine temperature currently limits the use of mid-grade (100 to 200ºC) heat.

In order for the primary advantage of thermal distillation (that heat, rather than high-exergy electricity, can be used for the energy of separation) to be realized for ZLD, innovative methods must be developed to allow the recycling of latent heat even for saturated solutions. This is evident as the minimum work of separation tops out at 7.7 kWh for extracting fresh water from a saturated (26.4 percent by weight, 0.1 mole fraction at 25ºC) NaCl) solution (Vane 2017), but the latent heat is 625 kWh/m3, some 80 times larger. Since the minimum work of separation is defined as a reversible thermodynamic process, it also specifies the minimum exergy input. This sets the minimum heat of separation, defined as $q_{min} = w_{min} (1 - T_0 / T)^{-1}$, where T_0 is the ambient or heat exhaust temperature, and T is the input temperature. The minimal heat of separation

provides another reason for the device to use higher-grade heat. Using heat at 75ºC, the theoretical minimal specific energy for any ZLD technique is 53.6 kWh/m3, but at 150ºC, the minimum drops to 26.0 kWh/m3.

Multiple-effect adsorption distillation could potentially solve all of these issues. The proposed adsorption distiller consists of a number of open-cycle adsorption stages connected in series, where the exhaust heat from an upper stage is used to drive the next stage. When a thermally driven heat pump can reuse prior-stage exhaust two or three times, it is referred to as a double- or triple-effect heat pump. We have eliminated the heat-pumping action to maximize the number of stages, creating a 16-effect heat pump that pumps no heat but is very efficient as a distiller. Based on an extensive literature and patent search, ours will be the first use of this method.

By keeping the evaporator and condenser essentially isothermal using a high heat transfer coefficient flat-plate condenser/evaporator, we are able to minimize the temperature difference needed to drive each stage. This design also keeps brine contact to only the flat-plate evaporator, which is easily disassembled and cleaned, mitigating the maintainability issue common to extended heat transfer surfaces in distillation plants.

The use of boiling thermosyphon heat transfer tubes to convey the heat of adsorption between beds eliminates forced convection circuits requiring pumping power. Reduction of pumping power is one method for achieving the very low specific electric energy, which is used only to pump solar thermal heat transfer fluid from the solar collectors and to return the small amount of boiling water in the thermosyphon tubes.

The specific energy we expect to achieve with the adsorption distiller is 23 $kWh_{thermal}$ + 0.1 $kWh_{electric}$ per cubic meter. Since this value is larger than the typical 3.6 $kWh_{electric}$ per cubic meter for RO (Ludwig 2010; Elimelech 2011), it is necessary to show that 23 kWh of thermal energy is more cost-effective than 3.5 kWh of electricity. Calculations show that solar thermal energy from our thermal collections system will cost only $0.003/kWh compared to the 2017 California industry sector average cost of electricity at $0.1273/kWh, 42 times lower in a state that is increasing its desalination capacity (EIA 2018), and 113 to 137 times lower than electricity prices in the Caribbean, where diesel is the primary fuel (McIntyre et al. 2016). Thermal storage in the form of hot water enables nighttime operations that will cost substantially less than electrical storage in batteries. The resulting thermal desalination device is economically competitive with RO. Our envisioned pilot demonstration product is shown in Figure 1.

GreenBlu's adsorption distillation also has a strong advantage when used in a crystallizer for ZLD desalination because the process operates by extracting water vapor without being in contact with the concentrated solution or precipitating slurry. Vapor pressure only decreases modestly with increased salinity, proportional to the mole fraction of salt in solution. This is evident, as the boiling point of a saturated salt solution is only elevated by 8.7ºC. This allows a vapor pump to operate the same on water of any salinity through slight modification of the brine temperature.

1.3.2 Overall Method

The schematic shown in Figure 2 shows two connected adsorption stages operating in the two modes, Heat Driven and Relaxation. Cyan arrows indicate vapor, blue arrows indicate liquid water, orange arrows indicate input water, and brown arrows indicate the bottom stream, which flows serially through each stage starting at the highest temperature. Each adsorption stage is composed of two beds with an evaporator/condenser between them that evaporates input water and condenses distillate. Vapor valves connect each bed to either the condenser or the evaporator, and each bed has both a grid of vertical copper tubes serving as a boiler/condenser to transfer heat between beds and a grid of hollow channels to transfer water vapor mass to/from the condenser/evaporator.

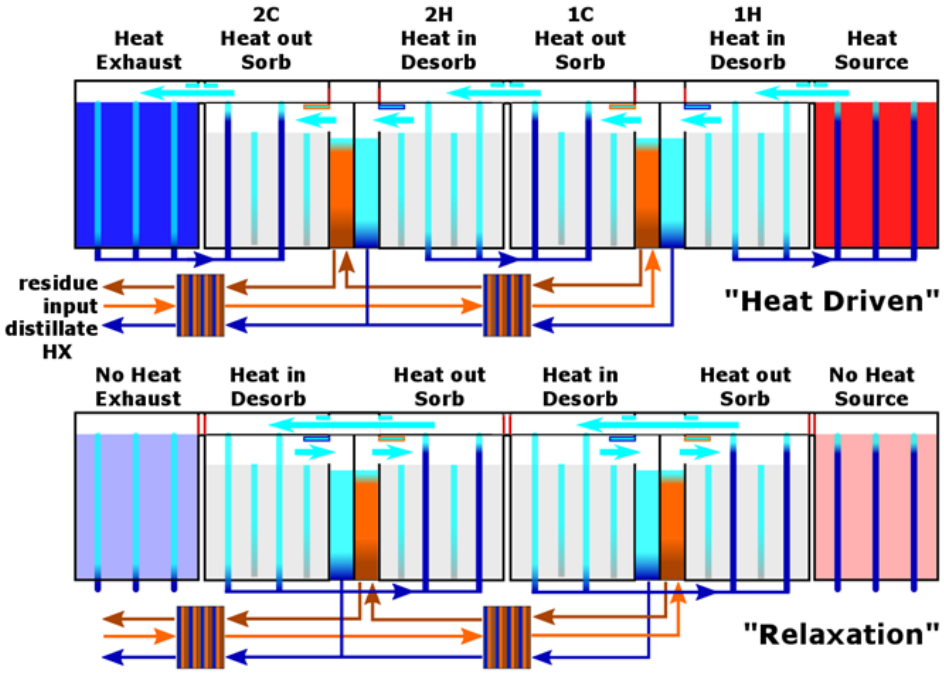

Figure 2. Schematic of proposed multiple-effect adsorption distiller

The heat transfer tubes are a closed-loop vapor system transferring just heat between adsorption beds using a working liquid/vapor. The boiler heat transfer coefficient is governed by nucleate pool boiling, and methods of boiling surface enhancements to minimize the boiling superheat can be used.

Cycle operations of a two-stage system are illustrated in Figure 2. In the heat-driven mode, the hot bed is heated by condensing vapor in the thermosyphon tubes generated by the heat source. This bed is open to the condenser, and the increase in temperature causes the adsorbent to desorb vapor, increasing the water vapor pressure and temperature in the condenser. This causes condensation and a transfer of the heat of vaporization to the input water in the evaporator. The next, colder bed is open to the evaporator, and its thermosyphon tubes transfer heat to the subsequent bed. The cooling of the subsequent bed causes it to adsorb vapor from the evaporator.

The heat of adsorption from this bed transfers to the next bed in the sequence until it reaches the equilibrium uptake at the lower temperature. The final bed exhausts adsorption heat to a condenser cooled by the final residue and cooling waters.

At the end of the heat-driven mode, the adsorption beds have become separated in temperature and uptake. The relaxation stage connects the hot and cold beds of each stage to allow them to come back to equilibrium. As heat transfers from the hot bed to cold bed, the cold bed desorbs vapor into the condenser, which in turn evaporates input water adsorbed by the hot stage.

This page intentionally left blank.

2 Technical Approach and Methods

2.1 Project Facility/Physical Apparatus

2.1.1 Design Criteria

Design criteria addressed five objectives, as identified below.

Objective 1: Optimize adsorbent module properties

The following adsorbent composition and constituent characteristics were examined:

1. Binder selection;
2. Internal reinforcement;
3. Graphite nanosheet size; and
4. Silica gel particle size.

The following adsorbent manufacturing techniques were examined:

1. Compression pressure vs. density;
2. Density vs. permeability; and
3. Compression procedure.

Objective 2: Design and construct benchtop-scale prototype bed

1. Produce a detailed prototype design; and
2. Fabricate prototype adsorption bed.

Objective 3: Test adsorption bed test stand

Objective 4: Create a conceptual design of commercial product

Objective 5: Interview customers for pilot, distiller, and crystallizer

2.1.2 Source Water

The objective was to improve the internal components of an adsorption distiller and demonstrate a proof-of-concept tabletop device. This was performed using both distilled water and a saturated sodium chloride solution.

2.1.3 Set-Up

The physical set-up and design for each of the adsorbent testing instruments will be shown and described in the corresponding methodology text in Section 2.2.

2.2 Methodology

2.2.1 Methods Used

2.2.1.1 Vapor Permeability Testing Apparatus

The vapor permeability of adsorbent prototypes is measured using differential pressure sensors and tubing of known conductance. This system, shown in Figure 3, contains two differential pressure sensors; the first sensor is exposed to the first and second tee connectors, while the second sensor is exposed to the second tee connector and to the atmospheric pressure. Compressed air from a standard compressor enters a pressure regulator which feeds into a low-pressure tee connector. From this connector, adaptors direct the compressed air to both the first of the two differential pressure sensors (via flexible plastic tubing) and a small capillary with a known conductance. Following its entry into the capillary, the air is then directed into a second tee connector. This connector feeds the air to both the adsorbent and the second of the two differential pressure sensors. At the point where the air is input into the center axis of the cylindrical adsorbent, it begins to diffuse radially outward through the material. Using a ratio calculation with the known conductance values and recorded differential pressures, it is possible to observe which adsorbent materials have more porous properties in relation to other tested prototypes.

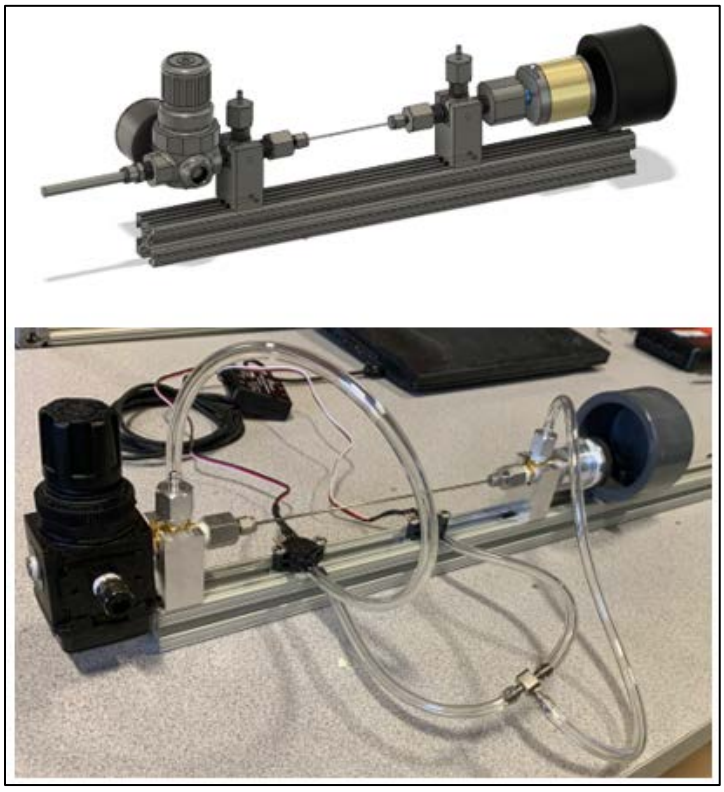

Figure 3. Vapor permeability testing apparatus as designed in CAD (top), and operational as-built (bottom)

In order to construct this apparatus, custom adaptors were manufactured in order to secure the apparatus to a solid aluminum rail and to connect its various components. First, channels were cut into aluminum blocks and screw holes were tapped into one side of the channel in order to secure the tee connectors in place at a set separation distance. These blocks were then secured to the aluminum rail with a tapped adapter, thus securing the location of the tee connectors with respect to one another. Following this, an adapter and plate were constructed and attached the adsorbent prototype to the apparatus in order to allow for compressed air to systematically flow through the material in a measurable way.

Figure 4. Annular adsorbent samples fabricated for permeability testing

2.2.1.1.1 Annular Sample Fabricated for Vapor Permeability

Annular samples (1.4 inches in diameter, 1 inch in length) have been fabricated using silica gel impregnated with a hydroscopic salt and mixed with graphite flakes, as shown in Figure 4. This adsorbent was compressed symmetrically in an aluminum slug and heated for 1 hour, giving us our adsorbent samples.

These samples were synthesized, varying certain parameters in order to test the effect of grain size, compression pressure, and binder on vapor permeability. Four different samples were made containing 100, 200, 400, and a combination of 100 and 200 mesh silica gel. A fifth sample was made using 100 mesh silica gel but compressed at twice the pressure. Additional samples were later made using different binders. Data for each sample were collected using our vapor permeability testing apparatus.

2.2.1.1.2 Rectangular Samples Fabricated for Thermal Conductivity

Two rectangular sample mold dies, with PID-controlled (proportional integral derivative) heating elements capable of binder-curing under pressure were constructed. The two dies are designed to compress either parallel or perpendicular to the testing direction for the thermal conductivity and toughness tests. A number of rectangular 5-cm-by-5-cm samples were constructed at 1-cm and 2-cm thicknesses using custom curing molds that allowed the direction of compression to be perpendicular to the direction of heat flux for the thermal conductivity tests.

2.2.1.1.3 Thermal Conductivity Testing Apparatus Design Methodology

Adsorbent thermal conductivity was tested using the ASTM C-518-98 methodology. Heat flux sensors were sourced from FluxTeq of Blacksburg, Virginia, and used in accordance with the ASTM procedures. Hot plates and cold plates were precision-machined using aluminum blocks, maintaining specified flatness requirements. Specified and constant pressure was maintained across the sample surface using springs compressed to equal lengths with shoulder bolts.

A conductivity sample tester using a pair of heat flux sensors has several advantages from a calibration perspective. By matching input with output fluxes through the sample, most loss mechanisms are simply known to be negligible. Figure 5 shows the testing apparatus nearing completion, with power supplies and the heatsinks and cooling fan for the cold plate visible.

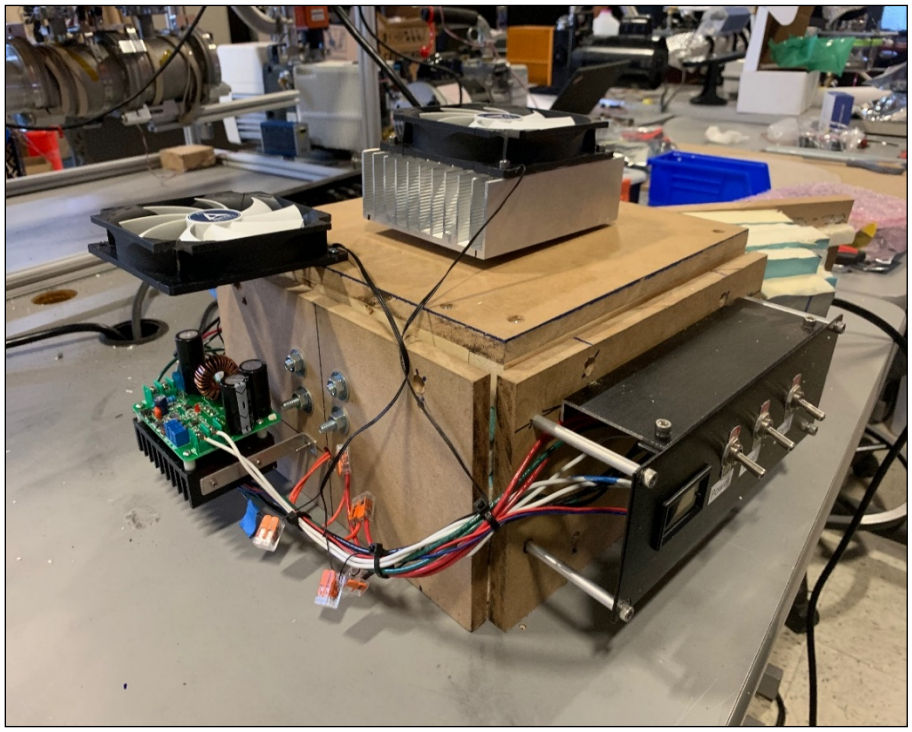

Figure 5. Thermal testing apparatus

During operation, a variable amount of power was used to heat the hot plate. The cold plate was cooled using a large heatsink with forced convection cooling. Custom Python software was used to log and chart heat flux and thermocouple data from a Phidget Hub and a 4x Thermocouple module, which was also used for measuring the output from the flux sensor. After reaching steady-state heat flux values, thermal conductivity was calculated using measured temperatures and sample thicknesses in the following equation:

$$k = \frac{qL}{\Delta T}$$

where k is the thermal conductivity (W/m*K), q is the heat flux (W/m^2), L is the sample thickness (m), and ΔT is the temperature difference (K) between the sample hot and cold surfaces.

2.3 Analysis

2.3.1 Analytical Background

2.3.1.1 Vapor Permeability Measurement Theory, Calculated Values, and Model Comparison

The vapor permeability of an annular adsorbent sample is calculated using a pressure drop ratio with a calibrated capillary tube. By conserving gas flux through the tube and the adsorbent sample using a serial flow path, we can compare the pressure drops through both flow restrictions to derive the permeability using Darcy's law and the Darcy-Weisbach empirical equation for pressure drop through a capillary tube.

Darcy's law describes the flow of fluid through a porous medium. In cylindrical coordinates for flow across an annulus, it can be written as:

$$Q = \frac{2\pi kL}{\mu}\frac{(p_2 - p_1)}{ln(r_2/r_1)} \qquad [1]$$

Where Q is the volumetric flow rate (m^3/s), L *(m)* is the length, μ is the dynamic viscosity of the fluid (for our test medium, air = 18×10^{-6} Pa·s), p (Pa) is the pressure on each side of the annulus, r (m) is the radii defining the annular region, and k (m^2) is the quantity of interest, the permeability of the medium.

The Darcy-Weisbach equation, an empirical expression for pressure drop due to capillary flow along a pipe, can be cast as follows for a circular tube:

$$\frac{\Delta p}{L} = \frac{f_D \rho Q^2}{2A^2 D} \qquad [2]$$

$$\langle v \rangle = \frac{Q}{A} \quad [3]$$

where $\langle v \rangle$ is the apparent velocity defined as the volumetric flow rate Q (m^3/s) divided by the area. For cylindrical annular geometry, area is defined by the log mean area (m^2), $A = (A_2 - A_1)/\ln({}^{A_2}/_{A_1})$. D is the hydraulic diameter, which is the ID of the capillary tube, ρ is the density of the flow medium (for air ρ=1.16 kg/m^3), Δp (Pa) is the pressure drop along the tube, and L (m) is the tube length. The Darcy friction factor can be estimated using the Blasius equation for smooth tubes as:

$$f_D = \frac{0.316}{Re^{0.25}} \quad [4]$$

$$Re = \frac{VD}{\nu} \quad [5]$$

where V is the flow velocity in the tube, D is the tube diameter, and $\nu=\mu/\rho$ (m^2/s) is the kinematic viscosity taking the ratio of the dynamic viscosity, μ, with the fluid density, ρ, with Re as the Reynolds number.

Combining all the above expressions and equating the volumetric flow rates gives the following equation comparing flow through a smooth capillary tube and a cylindrical annular porous medium:

$$Q = \left(\frac{2}{0.316}\right)^{4/7} \frac{A_{tube} D_{tube}^{5/7}}{\nu^{1/7}\rho^{1/7}L^{4/7}} \Delta p_{tube}^{4/7} = 2\pi \frac{k_{ads}L_{ads}}{\mu} \frac{\Delta p_{ads}}{ln({}^{r_2}/_{r_1})} \quad [6]$$

Eq. 6 allows us to solve for k_{ads} across the adsorbent by measuring Δp_{tube} and Δp_{ads} using the apparatus in Figure 5. However, for engineering purposes, the apparent velocity is a useful metric for estimating vapor flow into the adsorbent module, $\langle v \rangle$, defined for porous media as $\langle v \rangle = Q/\langle A \rangle$, where $\langle A \rangle$ is the log mean area, $A=2\pi L/ln(r_o/r_i)$, r_o and r_i being the outer and inner radii, respectively.

The experimentally-measured values can be compared to several models for pressure-driven gas transport in porous media summarized by Kawagoe et.al. (2016):

$$k_{B-K} = \frac{d_p^2}{150}\frac{\varepsilon^3}{(1-\varepsilon)^2}, Blake - Kozeny \quad [7]$$

$$k_{C-K} = \frac{d_p^2}{180}\frac{\varepsilon^3}{(1-\varepsilon)^2}, Carmen - Kozeny \quad [8]$$

$$k_{R-G} = \frac{d_p^2}{5.6}\frac{\varepsilon^{5.5}}{1.05}, Rumpf - Gupte \quad [9]$$

where d_p (m) is the effective average diameter of the packed particle comprising the porous medium, and ε (dimensionless) is the porosity and k (m^2) is the permeability of the porous medium.

2.3.1.2 Porosity Calculations

To calculate porosity, densities of the adsorbent are compared to the weighted average of its constituent component densities shown in Table 1. Using this method, a density measurement can be used to calculate porosity. Adsorbent porosities vary depending primarily on density but also on composition. Samples created for this project ranged between 0.49 and 0.07.

Table 1. Adsorbent constituents used to calculate densities

Constituent	Density (g/cm^3)
Silica Gel	0.70
Hygroscopic Salt	2.10
Graphite	2.15
Constituent #4	2.23
Constituent #5	1.4

2.3.2 Analytical Process

The temperature and heat flux data were collected using Phidget hardware and custom Python software. A time record of the data for each sample was collected over the course of 1/2 hour to 2 hours, depending on the time required for the test system to reach thermal equilibrium. The data were then analyzed using custom Python routines and test samples with known thermal conductivities (aluminum, stainless steel, and Delrin) to calibrate the system and determine the innate thermal resistances of the various thermal interfaces and system components, which can be generalized with the following equation:

$$\Delta T_{meas} = \Delta T_{TR} + \Delta T_k$$

This equation shows that the measured ΔT is a combination of a ΔT from the overall system thermal resistances and the ΔT due to the thermal conductivity of the sample, which is the quantity needed to determine the adsorbent sample thermal conductivity.

Calibration of the thermal interface resistance between the hot/cold plates and the adsorbent samples was found to be a strong factor in accurately determining the overall thermal conductivity. Because this thermal resistance varied considerably with the surface characteristics of the adsorbent, modified by properties such as silica gel particle size and graphite composition, we used high-conductivity thermal grease to provide a more uniform interface between the

adsorbent sample and the thermal system surfaces. As a result, the ΔT due to the thermal interface resistance from the fine-grit and coarse-grit samples dropped from about 5°C and about 10°C, respectively, to less than 1°C in each case. These results were further validated using a differential thickness measurement technique in which two samples of the same composition were made with a 1-cm and a 2-cm thickness. The difference in the total ΔT measured across each sample is precisely the temperature difference due to the sample thermal conductivity at 1-cm thickness (ΔT_k):

$$\Delta T_{k(1cm)} = \Delta T_{meas,2cm} - \Delta T_{meas,1cm}$$

After subtracting the calibrated system ΔT_{TR} from the various measured ΔT, we were able to determine the thermal conductivity values for the adsorbent samples, which are shown and discussed in Section 3.

3 Results and Discussion

3.1 Measured Adsorbent Thermal Conductivities

Figure 6 shows that increased graphite content has a strong effect on sample thermal conductivity. Our lowest graphite content samples still showed more than an order of magnitude higher thermal conductivity compared to pure silica gel granules. As expected, increasing the graphite content improved the thermal conductivity. Furthermore, we were able to refine our graphite production process to about double the improvement in overall thermal conductivity.

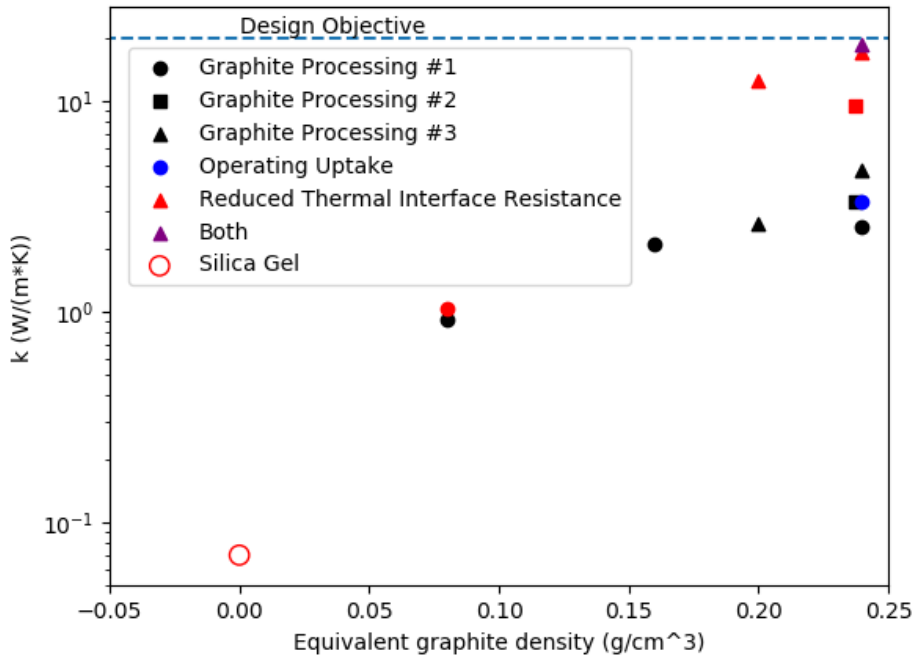

Figure 6. Adsorbent test sample thermal conductivity vs. graphite density

Once we applied thermal interface grease and accurately assessed the overall system thermal resistance, we were able to measure sample adsorbent thermal conductivities of about 17 W/(m*K), just shy of our design target of 20 W/(m*K). The graphite density noted on the X-axis is obtained through a combination of graphite weight percentage and overall sample density, which is related to the compression pressure during the binder curing process. Therefore, these data will be used in combination with the following permeability data to identify sample composition and production process parameters necessary to produce adsorbent material with target thermal conductivity, as well as target permeability.

3.2 Comparing Measured Permeability with Models

We collected vapor permeability data from adsorbent test samples with a variety of densities, compositions, and average silica gel particle size (see Figure 7). As expected from the porosity and permeability equations, permeability decreases with increased density and smaller particle size. However, while adsorbent samples without graphite tended to have higher densities, the permeability was also higher, likely due to increased overall porosity. The effect of adsorbent graphite content on porosity/permeability will need further characterization, especially in relation to the different graphite processing techniques, which can have an impact on average graphite particle size and flake geometry. With the porosity calculated, the permeability in Equation 6, k_{ads}, can be compared with the models in Equations 7 through 9.

3.3 Adsorbent Module Fabrication Techniques

We attempted multiple pre-assembly mixing techniques prior to compression for adsorbent module fabrication, where the adsorbent constituents were pre-mixed in various orders and under different conditions, such as water content, before being added to the compression/curing molds. The compression molds were created from standard aluminum alloy or stainless-steel tubing with a corresponding set of close-fitting pistons to compress the adsorbent constituents. Compression pressure was applied using a floor-standing 10-ton hydraulic press, with the pressure being continuously monitored throughout the process using a 1-ton button load cell from Phidget and custom Python software. The powder was compressed with the central heat transfer pipe in place to allow adsorbent bonding during the curing process.

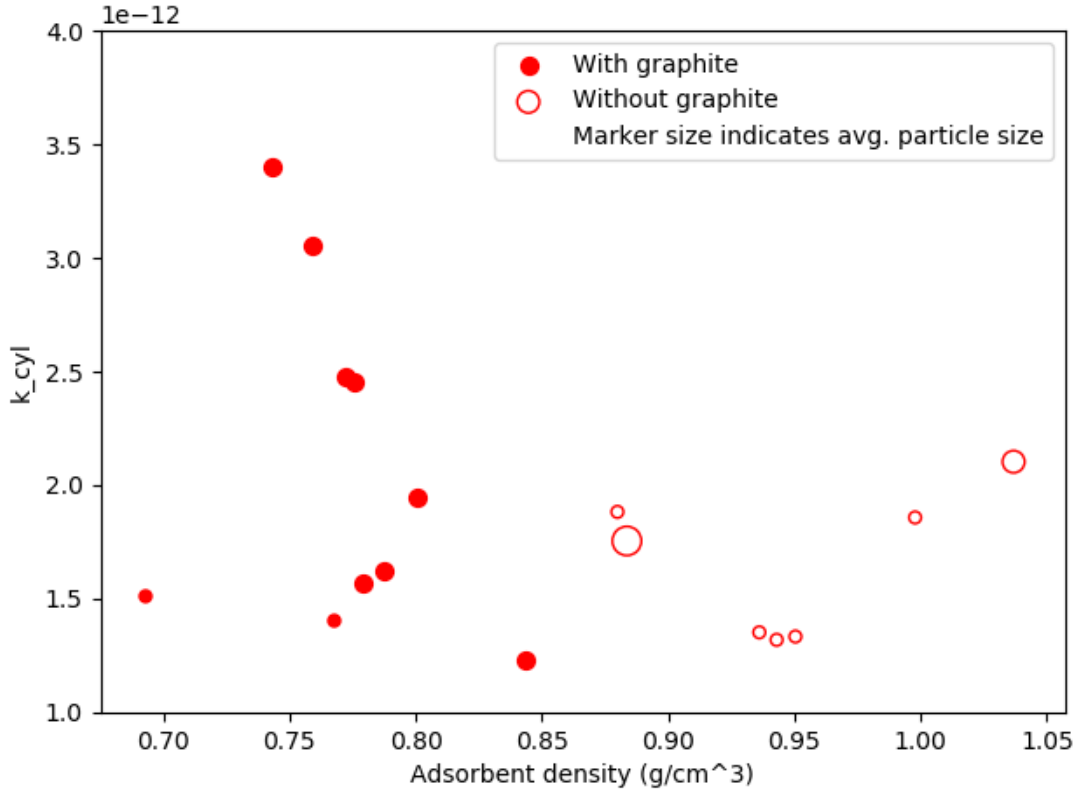

Figure 7. Adsorbent test sample vapor permeability vs. density with marker size related to adsorbent average particle size

The adsorbent curing process involved bringing the compression mold up to the appropriate temperature, while under pressure, and holding it at temperature for enough time such that the binder could melt and set throughout the full adsorbent volume. The mold temperature was monitored and controlled by standalone proportional integral derivative (PID) modules connected to AC solid-state relays. The relays used a variable duty cycle to apply 120 V of AC power to a set of cylindrical band heaters from Thermal Corporation that were spaced along the mold tubing. The final mold temperature and dwell time depended on the specifics of the binder used as well as the adsorbent composition. After this curing step, the adsorbent modules were ejected from the mold. If the central heat transfer pipe was insufficiently bonded to the adsorbent, the heat pipe was extracted and additional binder was applied. The heat pipe was then reinserted and the module was baked in a convection oven to cure the additional binder and re-adhere the pipe to the adsorbent cylinder.

Figure 8 shows the various components and results from our adsorbent module fabrication development. The pieces of the compression/curing molds (compression tubes, pistons, and band heaters) are shown in Figure 8a and Figure 8b shows various failed attempts in which either the adsorbent bonded to the compression tube or the soft copper central heat pipe buckled during the compression process. In fact, after various methods of attempting to strengthen or support the copper heat transfer pipe, we decided to switch to a thin-walled stainless steel heat transfer pipe

to eliminate this issue. This modification had the added benefit of reducing our projected unit cost by changing to a lower-cost heat pipe material. Figure 8c shows examples of successful adsorbent module fabrication. These adsorbent modules were then used as components in the proof-of-concept prototype discussed in the following section.

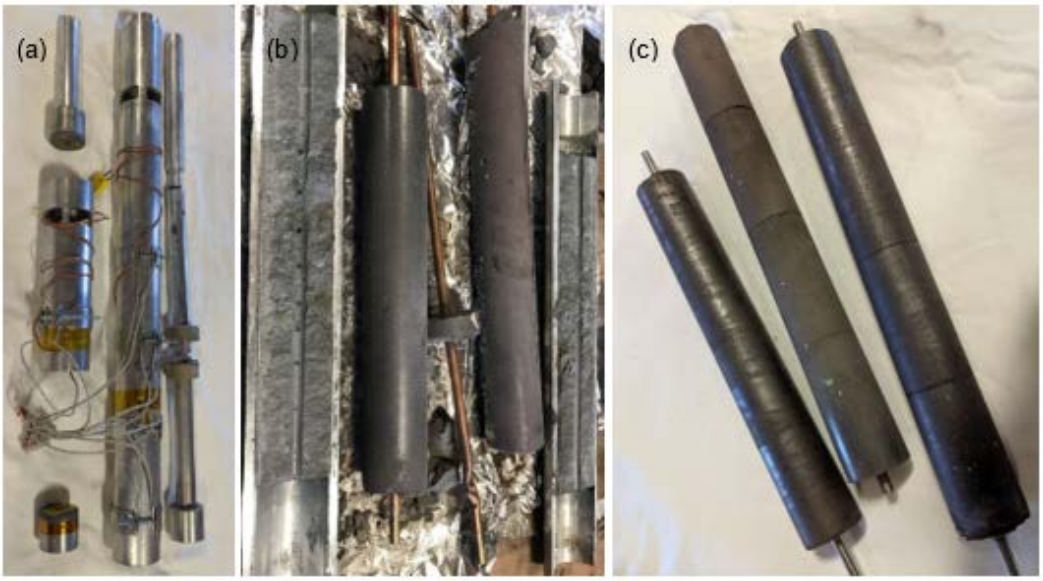

Figure 8. Adsorbent module fabrication progress: a) improved compressing and curing molds; b) initial unsuccessful attempts; and c) modules after multiple cycles in prototype

3.4 Adsorbent Bed Proof-of-Concept Prototype

We fabricated a prototype effect using four adsorbent rods in a single bed (see Figure 9). The adsorbent chamber was fabricated from an 18-inch-long, 12.5-inch inner diameter steel pipe. The inner diameter at each end of the pipe was turned on our lathe to produce a fine finish to O-ring seal the tube sheets, plenum plate, and caps. The tube sheets, plenum plate, and caps were fabricated in-house using both our three-axis CNC mill and the manual lathe. The adsorbent rods were sealed to the tube sheets using a custom Wilson-type O-ring seal. ISO-63 vacuum ports were made in the top cap to provide vapor access to the chamber and ReHEAT™ plenum. The lower liquid plenum was filled and drained via a national pipe thread (NPT) port. Vapor transfer tubes were standard KF-50 vacuum nipples and valves. The evaporation and condensation chambers were inverted 8-inch-diameter bell jars with polycarbonate covers. The covers had 2-inch NPT ports created for vapor transfer and feedthroughs for 1/4-inch copper condensation and stainless-steel evaporation coils.

Figure 9. Completed proof-of-concept adsorbent bed with evaporator and condenser

Four adsorbent rods weighing a total of 1.56 kg were used for this initial test; the passive mass was perhaps 30 times heavier. Switching from adsorption to desorption took approximately 20 minutes and switching from desorption to adsorption took 10 minutes. Closing valves between condenser, evaporator, and bed during this time allowed this transition time to be classified as non-active and subtracted from operational time.

The evaporator and condenser were operated using a serial loop with the same heating/cooling fluid, ensuring that they are near isothermal. Therefore, distillation does not occur between the evaporator and condenser when they are opened to each other (in practice, the system contains valves, so they are never directly connected) and requires the adsorbent bed to suck vapor from the evaporator and push vapor into the condenser. The adsorbent was operated from 50 to 95°C and the evaporator/condenser was held at 50°C. These limits were imposed by the external heating and cooling loops and the need to avoid condensation on all of the passive mass.

Two adsorbent rods composed of mid-range particle-size silica gel incipiently impregnated with hygroscopic salt was combined with graphite flakes, reinforcement, and a binder cured under pressure. The center tubes were made of stainless steel, after unsuccessful attempts using soft copper tubing which experienced buckling. Another two rods were fabricated using fine-grain silica gel with the same composition and curing process. Each rod was post-baked with additional binder along the center channel to adhere the stainless tube in place.

Analysis of the performance during active periods indicates that the system operated at approximately 1 mL/minute over 6 hours of operations. Since the total active mass was only approximately 1.3 kg, this extrapolated to a specific water production rate of 1.1 L/day/kg of

adsorbent, which is about 20 percent of the desired commercial production rate. This is an encouraging result so early in prototyping, since the performance of the adsorbent bed was almost certainly constrained by the heat transfer capacity of the evaporator and condenser coils, and the adsorbent itself was made using an unoptimized formulation. The adsorbent beds are designed to hold in excess of 20 adsorbent rods, which we will install in future prototype testing using a more optimized adsorbent rod.

3.5 Adsorbent Bed Test Stand

We fabricated a custom test stand to perform precision measurements of water uptake kinetics of the adsorbent (see Figure 10). The test stand is designed to measure temperature changes in adsorbent samples as well as vapor pressure in the chamber. Refinement of the test stand continued in parallel with adsorbent demonstrations with the prototype effect.

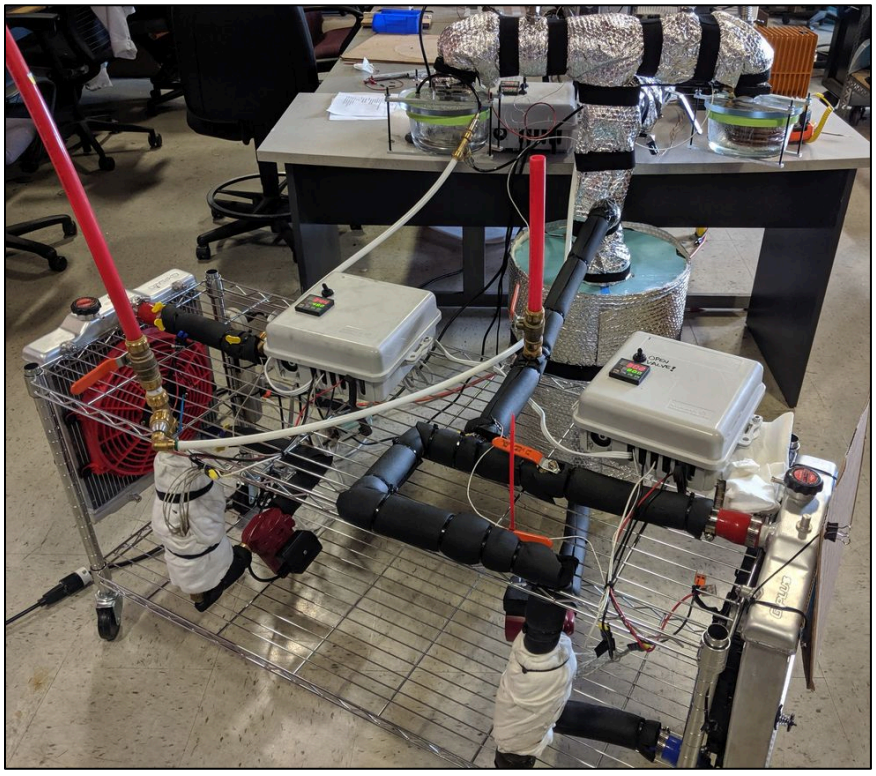

Figure 10. Prototype adsorbent bed connected to test stand

In order to operate a single adsorbent bed for testing, four PID feedback control loops had to be implemented to control the temperature of: 1) the bed chassis; 2) the vapor tee connecting the adsorption bed, evaporator, and condenser; 3) the evaporator/condenser; and 4) the adsorbent rods. The first two PID temperature loops ensured that the valves, transfers lines, and adsorbent bed chamber remained above the temperature of the evaporator and condenser. This ensured that

the adsorbent was responsible for water transfer, rather than condensation on the walls of the system.

The anticipated approach to this task was modified during the project. Initially, we had planned to fabricate two adsorption beds and couple them together using a commercial flat-plate evaporator/condenser to operate as a single effect. Our adsorbent recipe was still rapidly evolving when the adsorbent bed chamber fabrication was complete. We chose to reduce the technical and schedule risks associated with fabricating adsorbent rods for both chambers by converting to a single-bed effect. We achieved this by splitting the evaporator/condenser. By using a single heated/cooled water loop to operate both the evaporator and condenser at the same temperature, we could conclusively demonstrate that the adsorbent is a vapor pump capable of moving water from the evaporator to the condenser. Additionally, the measured equilibrium vapor isotherms shown in Figure 11 demonstrate that the adsorption/desorption cycle responds as predicted for the prototype system. As more water vapor is adsorbed by the modules, the saturated vapor pressure increases for a given temperature.

An added advantage of this approach was also the ability to demonstrate ZLD capabilities at this early stage. We were able to distill saturated NaCl brine in the separated evaporator and condenser. The completed bed with evaporator and condenser is shown in Figure 12 undergoing ZLD testing of a saturated NaCl brine.

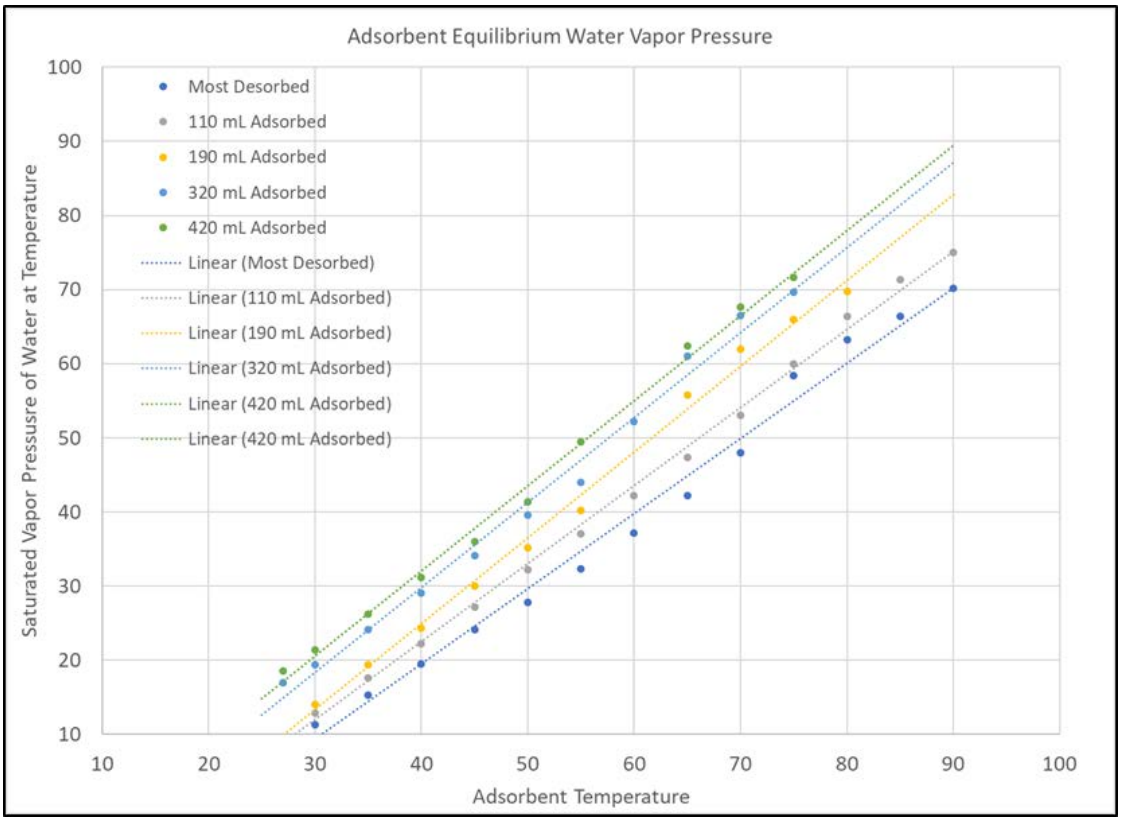

Figure 11. Equilibrium vapor pressure vs. temperature and uptake data from the adsorbent bed

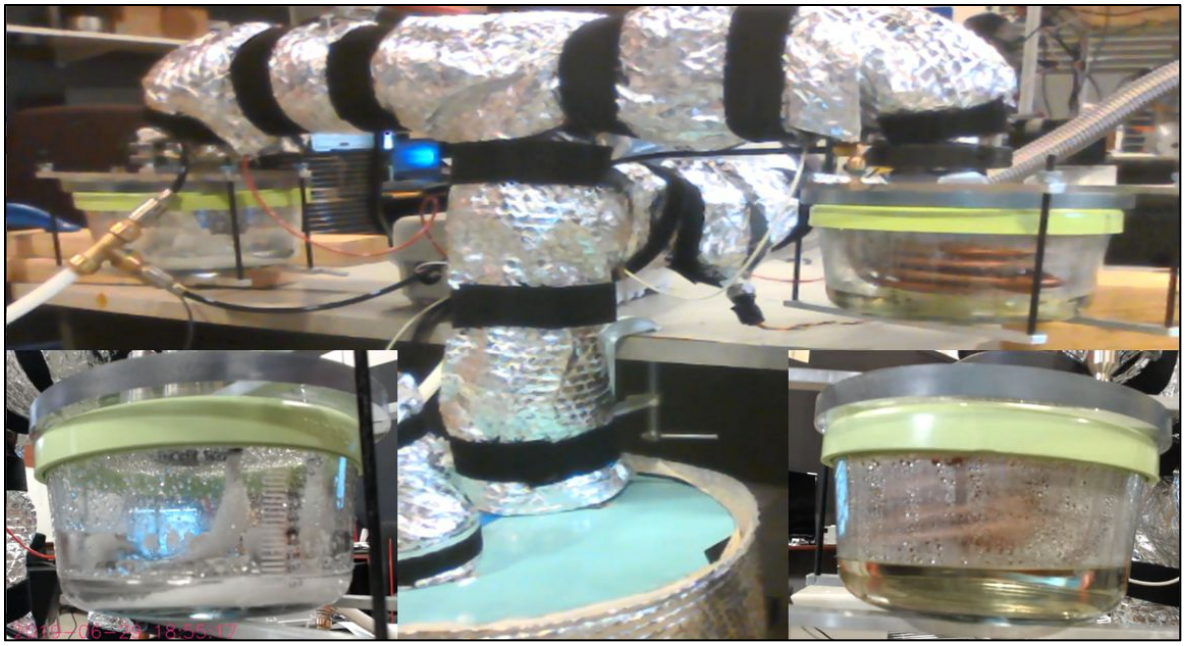

Figure 12. Completed adsorption bed connected to the test stand successfully distilling saturated NaCl brine using low-grade heat

3.5.1 Vapor Uptake Kinetics Testing

A separate test stand for measuring the adsorption and desorption rates of a single adsorbent module is shown in Figure 13. The apparatus consists of two chambers, a vapor generator, and a sample chamber. Each chamber is suspended from a digital scale and they are connected via a rigid vacuum line with isolation valves. PID heating loops independently controlled the temperatures of the vapor generator, transfer line, and sample chamber. An additional heated/cooled water loop controlled the temperature of the sample rod. Prior to testing, a vacuum pump was used to remove non-condensing gases from the system. The vacuum line was disconnected during test operations.

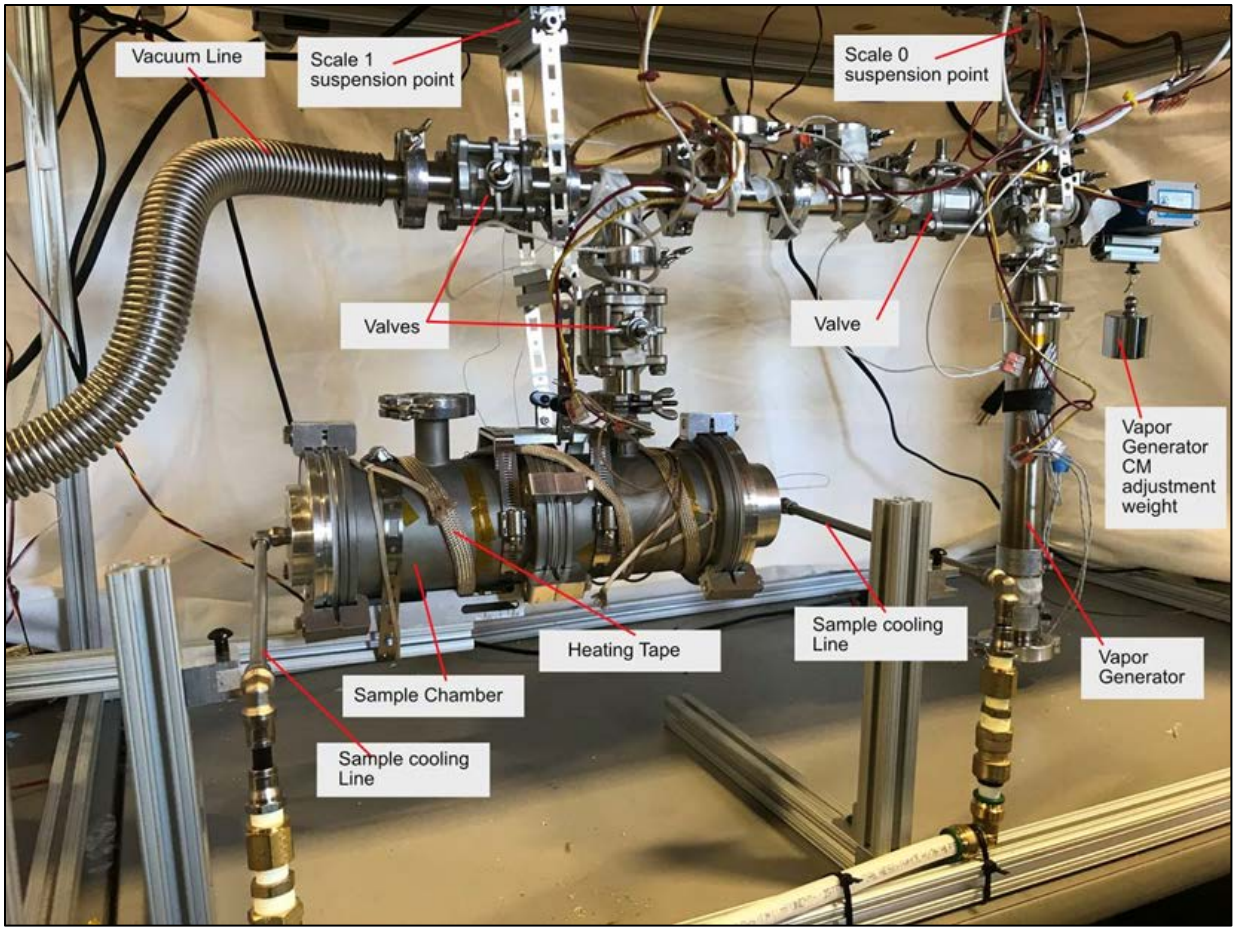

Figure 13. Adsorbent module uptakes kinetics testing apparatus

This testing apparatus used a flexible vacuum bellows in place of the rigid transfer line. The bellows was mounted in a four-bar mechanism to prevent the chamber positions from shifting with pressure and introducing errors into the scale readings. However, the thermal expansion of the bellows caused the four-bar mechanism to deflect vertically, introducing errors in scale readings through an induced torque. We replaced the bellows with a rigid line to eliminate this systematic error. The rigid line can still couple the scale readings through torques induced by transferring mass from the vapor generator to the sample chamber or vice versa. Figure 14 shows how the torques induce errors, and our solution to eliminate them. We used suspended masses to adjust the positions of the centers of mass of the vapor generator and sample chamber. When the centers of mass coincided with the points of suspension, mass transferred from one chamber to the other had no lever arm to generate a torque.

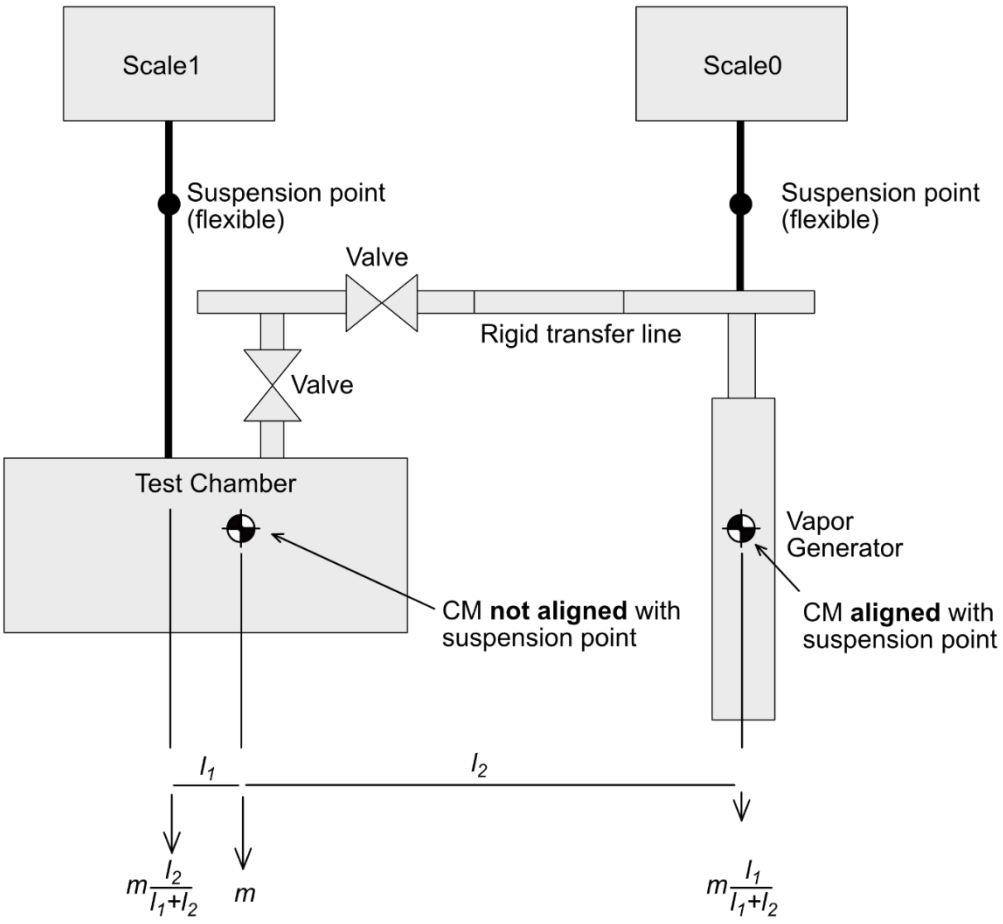

Figure 14. Updated approach to balancing vapor uptake testing chamber. Careful calibration and suspension from center of mass on each scale will eliminate influence of torques in the system on water mass measurements.

An initial test of an adsorbent sample is shown in Figure 15. The plot shows a comparison between temperature data, when an adsorbent module was present (solid lines) in the test chamber, and the baseline case, when only a copper tube was present (dashed lines). The most important thing to note in this test is that the exothermic reaction of water vapor being adsorbed by the adsorbent is clearly visible as the temperature of the module rises above the temperature of the water evaporating in the vapor generator. When the adsorbent is not present, the copper tube tracks the temperature of the vapor generator. This test was conducted without cooling the adsorbent and some systematic effects are not yet fully compensated. However, our initial estimate of water vapor uptake is 5 to 7 percent of the mass of active adsorbent. The total time required for this uptake cannot be determined from this test because the sample chamber was below the vapor generator temperature. When the test began, vapor very rapidly condensed on the chamber walls and then re-evaporated as the as vapor was adsorbed by the sample on longer timescales.

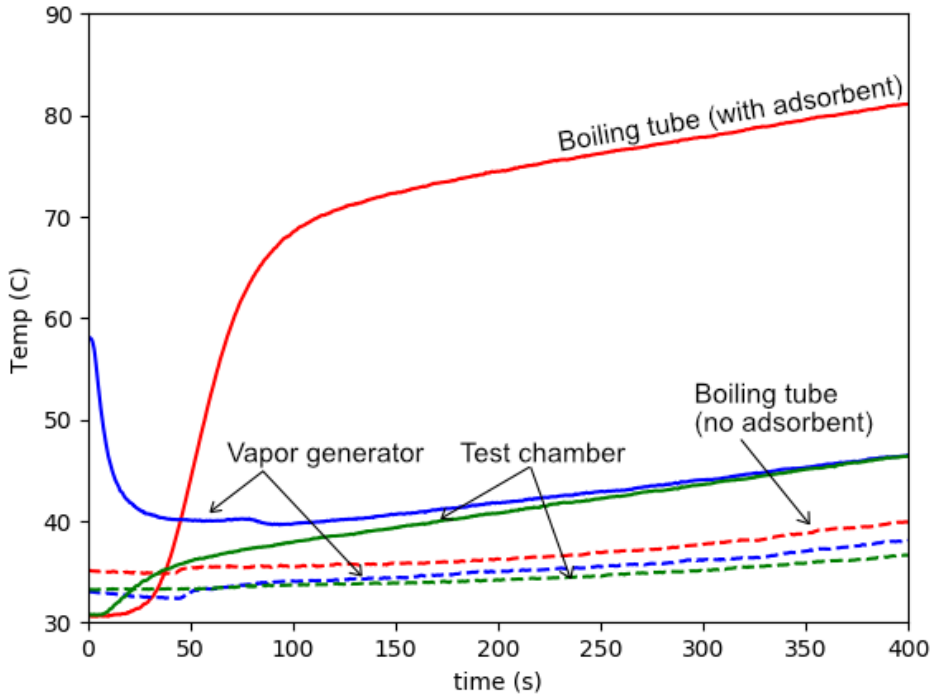

Figure 15. Temperature changes during an initial test of the uptake kinetics testing chamber

A new testing protocol was developed to resolve the time evolution of the adsorption of water vapor. The test chamber and transfer lines were to be held at the same temperature as the vapor generator to prevent condensation. This protocol was used successfully in the prototype effect. Additional testing with the test stand will resume when the current adsorbent rods are removed from the prototype effect. Testing of adsorbent properties, such as equilibrium vapor pressure versus temperature, were performed by instrumenting the prototype effect with a pressure sensor.

3.6 Adsorbent Bed Proof-of-Concept Design and Construction

The preliminary design for a commercial distiller has been completed. A collection of images from the design is shown in Figure 16. The distiller uses 16 stages, each of which is composed of two adsorbent beds and an evaporator/condenser sandwiched between the beds. Each bed has three valves. Two valves switch the bed between the condensing or evaporating ports of the evaporator/condenser and one valve controls working vapor to enter or leave the thermosyphon tubes of the adsorbent modules (this is referred to as the ReHEAT™ valve in the figure). The beds have three plenums. Below the bed is a liquid plenum to fill or remove water from the thermosyphon tubes. At the top of the bed is the plenum for ReHEAT™ working vapor to enter or exit the adsorbent module thermosyphon tubes. The main cavity which houses the adsorbent is the third plenum. Each bed is roughly 1 m by 2 m by 0.5 m and contains approximately 1,000 adsorbent modules that are the same dimensions as we fabricated and tested for this project. The entire distiller therefore contains approximately 32,000 adsorbent modules.

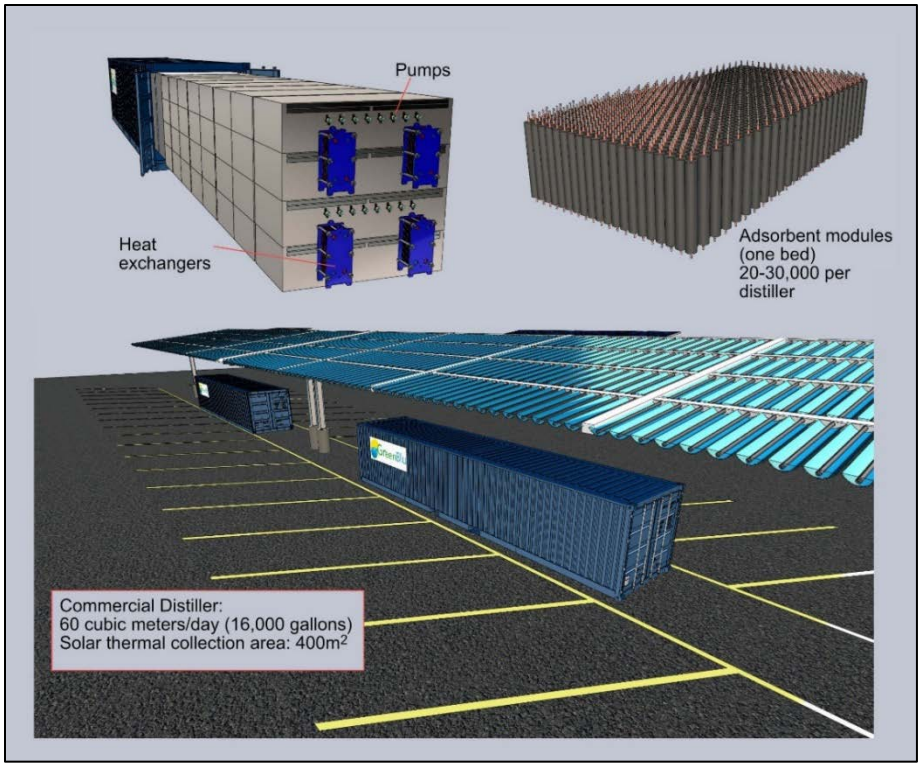

Figure 16. Conceptual design and rendering of commercial adsorption distiller

Each of the 32 beds contains approximately 325 kg of active adsorbent undergoing alternating adsorb and desorb cycles. This produces 60 cubic meters of water per day using approximately 23 kWh/m3 of thermal energy and 0.1 kWh/m3 of solar electricity.

Heat for the distiller is provided by 440 m^2 of solar thermal collectors. This is equivalent in area to roughly 40 parking spaces. The distiller is projected to produce 60 m^3 per day (16,000 gallons) assuming a solar insolation of 5 kWh/m^2/day, which is valid for much of the United States. Nighttime operation is powered by approximately 13 cubic meters of pressurized and sealed hot water stored at 10 atmospheres with a working temperature range of 180°C to 150°C.

4 Conclusions and Recommendations

4.1 Conclusions

Significant advances in adsorption distillation have been made as part of this project. Each major task within the project was completed successfully and produced advancement within each category. A summary of project outcomes is summarized below for each major objective.

Objective 1: Optimize adsorbent module properties

The project advanced the optimization of the adsorbent with respect to constituent characteristics and composition. Experiments with various constituent properties, including particle sizes, were conducted to examine their effect on adsorbent performance.

Development of adsorbent for commercialization was advanced by improving mechanical structure and durability. Module manufacturing techniques were prototyped and developed, examining the effect on density versus compression pressure. Permeability versus density was measured using a custom apparatus, and thermal conductivity versus composition and density was measured. Manufacturing methods compatible with industrial scale-up were explored.

Objective 2: Design and construct benchtop-scale prototype bed

A proof-of-concept adsorption bed prototype was designed and constructed using the same size adsorption modules as designed for the commercial product. The adsorption bed uses separate chambers for heat of adsorption transfer from the input solution and successfully tested plenums and manifolds necessary for operations. A successful test at this small scale inspires confidence for the scale-up to the next larger iteration of a prototype adsorption bed.

Objective 3: Test adsorption bed test stand

The adsorbent bed has successfully distilled a saturated NaCl solution, proving the efficacy of adsorption distillation for ZLD applications. During the test, a test stand comprising four independent feedback temperature control loops was integrated to control the temperature of the passive and active elements in the bed, as well as the temperature of the vapor plumbing between elements to prevent condensation. Brine and distillate were maintained at the same temperature as to require the adsorbent bed to actively pump vapor from the evaporator and force vapor into the condenser. This successful test culminated with achieving approximately 20 percent of the specific water production rate desired in the commercial product.

Objective 4: Create a conceptual design of commercial product

A conceptual design of a containerized multiple-effect solar-powered adsorption distiller was successfully completed. The design draws from the results obtained from other tasks and the successful prototype bed. Important parameters of the conceptual design are described in Table 2.

Table 2. Key specifications of the conceptual design

Specification	Value
Water production	60 m^3/day
Solar collection area	410 m^2
Specific Energy	23 $kWh_{thermal}$ + 0.1 $kWh_{electric}$
Energy Storage	Pressurized hot water storage
Form factor	40ft ISO Intermodal Container
Levelized Cost of Water	<$1.00/$m^3$

Objective 5: Interview customers for pilot, distiller, and crystallizer

Potential stakeholders, from industrial and commercial business customers to public utility executives to desalination project developers, were interviewed for their feedback to GreenBlu's technology. The response was overwhelmingly positive, with many respondents highly interested in pursuing a piloting opportunity or future sales. Several interviewees indicated they viewed GreenBlu's products as game-changing and welcomed its potential to disrupt the desalination and ZLD markets. Specifically, after discussions with multiple potential end-users, ZLD was identified as a high-demand element which would enable and expand currently-stalled inland desalination projects lacking viable brine management options. A desalination project developer indicated that the development of affordable and sustainable ZLD brine management would open up vast reserves of inland brackish groundwater in the southwest United States to help sustain agriculture and urban usage.

4.2 Recommended Next Steps

GreenBlu has accelerated the commercialization of its patented VADER™ multiple-effect adsorption distiller and crystallizer under multiple awards through the U.S. Department of Energy. The company is also in discussions with equity investors to secure additional funding for the commercialization of its products.

References

Citation in Text	Bibliographic Reference
Al-Ahmad and Abdul Aleem 1993	Al-Ahmad, M. and F. A. Aleem. 1993. "Scale Formation and Fouling Problems Effect on the Performance of MSF and RO Desalination Plants in Saudi Arabia." *Desalination* 93, pp. 287-310.
Aristov et al. 1996	Aristov, Y. I., M. M. Tokarev, G. Restuccia, and G. Cacciola. 1996. "Selective Water Sorbents for Multiple Applications, 2. CaCl2 Confined in Micropores of Silica Gel: Sorption Properties." *Reaction Kinetics and Catalysis Letters* 59, pp. 335-342.
EIA 2018	U.S. Energy Information Administration. 2018. Table T5.c, EIA Electricity Reports. Electric Sales, Revenue, and Average Price. Available online at https://www.eia.gov/electricity/sales_revenue_price/pdf/table5_c.pdf (last accessed 9/30/2019).
Elimelech 2011	M. Elimelech. 2011. "The Future of Seawater Desalination: Energy, Technology, and the Environment." *Science* 333, No. 6043, pp. 712-717. DOI: 10.1126/science.1200488
Famiglietti 2014	Famiglietti, J. S. 2014. "The Global Groundwater Crisis." *Nature Climate Change* 4, pp. 945–948.
Freni et al. 2007	Freni A, F. Russo, S. Vasta, M. Tokarev, Y. I. Aristov, and G. Restuccia. 2007. "An Advanced Solid Sorption Chiller Using SWS-1L." *Applied Thermal Engineering* 27, No. 13, pp. 2200-2204.
GAO 2014	U.S. Government Accountability Office. 2014. *Freshwater: Supply Concerns Continue, and Uncertainties Complicate Planning*. GAO-14-430.
IEA-ETSAP and IRENA 2012	International Energy Agency – Energy Technology Systems Analysis Programme and International Renewable Energy Agency. 2012. "Water Desalination Using Renewable Energy." *Technology Brief*. March 2012.
Jones et al. 2019	E. Jones, M. Qadir, M.T.H. van Vliet, V. Smakhtin, and S. Kang. 2019. "The State of Desalination and Brine Production: A Global Outlook." *Science of The Total Environment* 657 pp. 1343-1356.
Kawagoe et al. 2016	Kawagoe, Y., T. Oshima, K. Tomarikawa, T. Tokumasu, T. Koido, and S. Yonemura. 2016. "A Study on Pressure-Driven Gas Transport in Porous Media: from Nanoscale to Microscale." *Microfluidics and Nanofluidics* 20, 162. DOI 10.1007/s10404-016-1829-8.
Kim et al. 2015	Kim, D., G. L. Amy, and T. Karanfil. 2015. "Disinfection By-Product Formation during Seawater Desalination: A Review." *Water Research* 81, pp. 343-355.
LIGTT 2014	Institute for Globally Transformative Technologies, Lawrence Berkeley National Lab. 2014. *50 Breakthroughs: Critical Scientific and Technological Advances Needed for Sustainable Global Development*. Available online at https://ligtt.org/sites/all/files/page/50BTs-List.pdf (last accessed September 12, 2016).

Citation in Text	Bibliographic Reference
Ludwig 2010	Ludwig, H. 2010. "Energy Consumption of Reverse Osmosis Seawater Desalination — Possibilities for its Optimisation in Design and Operation of SWRO Plants." *Desalination and Water Treatment* 13, pp. 13-25.
McIntyre et al. 2016	McIntyre, A., A. El-Ashram, M. Ronci, J. Reynaud, N. X. Che, K. Wang, S. A. Mejia, and M. S. Lutz. 2016. "Caribbean Energy: Macro Related Challenges." *IMF Working Paper* No. 16/53.
Mekonnen and Hoekstra 2016	Mekonnen, M. M., and A. Y. Hoekstra. 2016. "Four Billion People Facing Severe Water Scarcity." *Science Advances* 2, No. 2. DOI: 10.1126/sciadv.1500323
Perez-Gonzalez et al. 2012	Perez-Gonzalez, A., A. M. Urtiaga, R. Ibanez, and I. Ortiz. "State of the Art and Review on the Treatment Technologies of Water Reverse Osmosis Concentrates." *Water Research* 46, pp. 267-283.
Roberts 2014	Roberts, A. G. 2014. "Predicting the Future of Global Water Stress." *MIT News*. January 9, 2014.
SBC 2014	SBC Energy Institute. 2014. Leading the Energy Transition Factbook: Introduction to the Water and Energy Challenge. Available online at https://www.idaea.csic.es/sites/default/files/Introduction-to-the-water-and-energy-challenge-SBC.pdf (last accessed July 10, 2020).
Thiel et al. 2015	Thiel, G. P., E. W. Tow, L. D. Banchik, H. W. Chung, and J. H. Lienhard. 2015. "Energy Consumption in Desalinating Produced Water from Shale Oil and Gas Extraction." *Desalination* 366, pp. 94–112.
Thu et al. 2015	K. Thu, Y-D. Kim, M. W. Shahzad, J. Saththasivam, and K. C. Ng. 2015. "Performance Investigation of an Advanced Multi-Effect Adsorption Desalination (MEAD) Cycle." *Applied Energy* 159, pp. 469–477.
Tibbetts 2002	Tibbetts, J. 2002. "Coastal Cities: Living on the Edge." *Environmental Health Perspectives* 110, pp. 674-681.
Tularam and Ilahee 2007	Tularam, G. A. and M. Ilahee. "Environmental Concerns of Desalinating Seawater using Reverse Osmosis." *Journal of Environmental Monitoring* 9, pp. 805-813.
2030 Water Resources Group 2009	2030 Water Resources Group. 2009. *Charting Our Water Future; Economic Frameworks to Inform Decision-Making*.
Vane 2017	Vane, L. 2017. "Water Recovery from Brines and Salt-Saturated Solutions: Operability and Thermodynamic Efficiency Considerations for Desalination Technologies." *Journal of Chemical Technology and Biotechnology* 92, No. 10, pp. 2506-2518.
Water in the West 2016	Water in the West, Center for Ocean Solutions, Monterey Bay Aquarium, and The Nature Conservancy. 2016. "Marine and Coastal Impacts of Ocean Desalination in California." *Dialogue Report*. Water in the West, Stanford University.

Metric Conversions

Unit	Metric equivalent
1 gallon	3.785 liters
1 gallon per minute	3.785 liters per minute
1 gallon per square foot of membrane area per day	40.74 liters per square meter per day
1 inch	2.54 centimeters
1 million gallons per day	3,785 cubic meters per day
1 pound per square inch	6.895 kilopascals
1 square foot	0.093 square meters
°F (temperature measurement)	(°F–32) × 0.556 = °C
1 °F (temperature change or difference)	0.556 °C